Received December 6, 2021, accepted December 28, 2021, date of publication January 5, 2022, date of current version January 14, 2022.

*Digital Object Identifier 10.1109/ACCESS.2022.3140440*

# Geometry and Topology Optimization of Switched Reluctance Machines: A Review

**MOHAMED ABDALMAGID[1,2], (Graduate Student Member, IEEE), EHAB SAYED[3], (Member, IEEE), MOHAMED H. BAKR[1], (Senior Member, IEEE), AND ALI EMADI[1], (Fellow, IEEE)**

[1]Department of Electric and Computer Engineering, McMaster University, Hamilton, ON L8S 4S4, Canada
[2]Department of Power Electronics and Energy Conversion Systems, Electronics Research Institute, Cairo 12622, Egypt
[3]Enedym Inc., Hamilton, ON L8P 0A1, Canada

Corresponding author: Mohamed Abdalmagid (abdelm47@mcmaster.ca)

This work was supported in part by the Natural Sciences and Engineering Research Council of Canada (NSERC).

**ABSTRACT** Switched reluctance machines (SRMs) have recently attracted more interest in many applications due to the volatile prices of rare-earth permanent magnets (PMs) used in permanent magnet synchronous machines (PMSMs). They also have rugged construction and can operate at high speeds and high temperatures. However, acoustic noise and high torque ripples, in addition to the relatively low torque density, present significant challenges. Geometry and topology optimization are applied to overcome these challenges and enable SRMs to compete with PMSMs. Key geometric design parameters are optimized to minimize various objective functions within geometry optimization. On the other hand, the material distribution in a particular design space within the machine domain may be optimized using topology optimization. We discuss how these techniques are applied to optimize the geometries and topologies of SRMs to enhance machine performance. As optimizing the machine geometry and material distribution at the design phase is of substantial significance, this work offers a comprehensive literature review on the current state of the art and the possible trends in the optimization techniques of SRMs. The paper also reviews different configurations of SRMs and stochastic and deterministic optimization techniques utilized in optimizing different configurations of the machine.

**INDEX TERMS** Deterministic optimization, geometry optimization, stochastic optimization, switched reluctance machines, topology optimization.

## I. INTRODUCTION

Switched reluctance machines (SRMs) are now attractive choices for various applications such as electric vehicles and hybrid electric vehicles [1], [2], wind power generation applications [3], and micro-electromechanical systems (MEMS) [4], [5]. The reason is that they have a simple and rugged structure without any magnets or windings on the rotor part [6]. The lack of the PMs and the winding on the rotor allows the machine to run at high temperatures and high speeds [7]. It also reduces the rotor weight, which increases the torque-to-inertia ratio of the machine and improves the dynamic performance as compared to the induction machines (IMs) and PMSMs [8], [9]. Additionally, the lack of rare-earth PMs from the machine design makes SRMs a low-cost substitute to PM-based machines.

The associate editor coordinating the review of this manuscript and approving it for publication was Wei Xu.

SRMs also use concentrated winding for the coils of phases, which decreases the assembly and replacement costs. It also decreases the electromagnetic coupling between the machine phases, which improves the SRMs fault-tolerance capability [10]. These advantages improve the machine's reliability and make SRMs a reliable option for different applications [11]–[13].

However, the doubly salient nature of SRMs structure introduces challenges such as high torque ripples and high acoustic noise and vibrations [14]. The acoustic noise and vibrations are mainly due to the high radial and axial forces for the radial and the axial SRMs configurations, respectively [14]–[19]. Moreover, SRMs are characterized by a small air gap thickness between rotor and stator, which requires a precise manufacturing tolerance [20]. The machine drive requires uncommon converters, which is another weak point of the machine drive system [15]–[17].

Extensive research was performed to overcome these disadvantages and improve the machine's static and dynamic

performance [1]. New configurations are developed, and optimization procedures are applied to enhance the machine's performance. Geometry and topology optimization are used to overcome these disadvantages and allow SRMs to compete with PMSMs. In Geometry optimization, key design parameters of the motor geometry are optimized to achieve various design objectives. On the other hand, the material distribution in a particular design space within the machine domain is optimized to improve machine performance through topology optimization.

In this work, different SRM configurations are illustrated. The merits, demerits, and application of each of these configurations are described. Also, an effort is made to present a comprehensive literature review of the deterministic and stochastic optimization methods used for improving the different performance indices of SRMs. A comprehensive survey of the geometry optimization and topology optimization methods used for SRM design in the literature is presented through this work. Finally, the convolution neural network optimization technique used in other electric machines is illustrated as a trend in the topology optimization of electric machine design. The latter technique was not used for SRM optimization yet; however, this technique's efficiency in saving optimization time and computational load motivates the authors to present it in this paper as a potential technique that could be used for SRM topology optimization to reduce the computational optimization burden.

The paper is arranged as follows. Section II classifies various SRMs configurations and illustrates the applications, advantages, and disadvantages of each configuration. The different performance measures used in SRMs' optimization as objective functions are reviewed in Section III. Section IV presents the existing deterministic and stochastic optimization methods used for the optimization of electric machines. The geometry optimization of SRMs and the recent studies in this area to improve the performance of SRMs are discussed in Section V. In Section VI, the topology optimization methods used for enhancing the performance of SRMs are discussed. In Section VII, the convolution neural network (CNN) optimization technique used in other electric machines is illustrated as a potential trend in the topology optimization of SRMs. Finally, the trends and opportunities in the SRMs design and optimization are outlined in Section VIII.

## II. MAIN CONFIGURATIONS OF SRMs

SRMs can be categorized based on the motion type to linear and rotary configurations and based on the flux-flow orientation to radial and axial flux machines. There are various stator/rotor pole combinations of SRMs. The number of rotor and stator teeth, in addition to the number of phases, are determined to ensure a feasible design of SRMs [21]. Most of the possible design stator/rotor poles combinations were illustrated in [22] and [23]. The selection of the machine configuration and stator/rotor poles combination defines the performance and depends significantly on the application [23]. A classification of SRMs based on the configuration is shown in Fig. 1.

The number of poles and the flux direction determine the configuration of the SRM. The classical and well-known designs of the SRMs adopt the radial flux machine with a rotor number of poles less than the stator number of poles. These configurations are characterized by high torque ripples and high acoustic noise and vibrations [24]. This issue is solved by increasing the number of rotor poles to be higher than the number of stator poles. The torque density and the noise-causing radial/axial forces can be improved by selecting the number of the rotor poles to be higher than that of the stator poles [24]–[26]. However, the high number of rotor poles increases the operating frequency, which increases the machine core loss [27]. It also decreases the conduction period per phase, which results in more switching losses and requires high-cost position sensors [28], [29]. SRMs with a higher number of rotor poles are therefore more suitable for low-power and low-speed applications [23]. On the other hand, machines with a lower ratio of the rotor to stator poles are selected for better utilization of the volt-ampere converter rating [23].

In axial-flux SRMs (AFSRMs), the flux travels axially between the stator and rotor. Due to the relatively shorter flux path, AFSRMs have a higher power density than radial-flux SRMs [30]. AFSRMs can be classified into three main categories. These categories include single-stator single-rotor (single-sided) machine, two-airgap (double-sided) machine, and multi-stack machine. The single-sided is the simplest AFSRM structure [31], [32]; however, the disadvantage of this configuration is the imbalance between the axial forces of the stator and rotor [33], [34], which produces high acoustic noise and needs to be accommodated in the bearing design [18]. The problem of the unbalanced axial force is solved by Double-sided AFSRMs configuration [35]. The Double-sided AFSRMs have a higher torque density; however, the structure is more complex than the single-sided AFSRMs configurations [35]–[37]. The multi-stack designs of the AFSRMs are much more complex structures as they should have at least three rotors or three stators [18]. The advantage of the multi-stack AFSRMs is the higher power and torque densities [18]. There are two types of multi-stack AFSRMs, either having equal or different numbers of rotors and stators. The equal number of rotors and stators has the disadvantage of unbalanced axial force; however, this configuration has a higher torque density than the multi-stack AFSRMs with different rotors and stators [18].

The linear SRMs configuration has a different function as it provides a linear motion. Linear SRMs (LSRMs) have a similar structure to rotary SRMs, except that the stator and rotor have a linear form. They consist of a stator (stationary part) and a translator (moving part) [38]. LSRMs configurations comprise planar and tubular designs. The planar linear SRMs has two types the unilateral-type and the Bilateral-type. The unilateral type has the advantage of the simple structure as it consists of one translator and one stator.

However, the unilateral-type main disadvantage is the high unbalanced axial forces between the stator and the translator, causing immense friction between both parts. The friction potentially reduces the machine lifetime [39]. This disadvantage is solved by the Bilateral-type but with a more complex structure consisting of two stators and a single translator [40]. All the planar Linear SRMs have a common disadvantage of having transversal cuts and uniform magnetic field distribution in the transversal direction. This problem is solved by the tuber-type Linear SRMs that a tuber shape stator with no transversal cuts [41], [42]. However, A precise shaft installation is needed to prevent unbalanced radial magnetic forces [43].

In this section, the construction, advantages, disadvantages, and applications of the different SRM configurations are presented. The rotary SRMs are discussed in subsection A, while the linear SRMs are illustrated in subsection B.

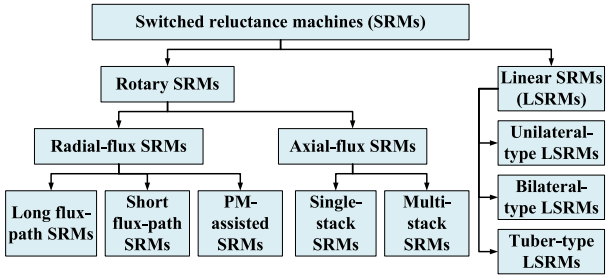


**FIGURE 1.** Main configurations of SRMs.

### A. ROTARY SRMs

As illustrated in Fig. 1, rotary SRMs are divided into two configurations: radial-flux SRMs and axial-flux SRMs. The radial-flux SRMs are divided into three types: long-flux-path SRMs, short- flux-path SRMs, and PM-assisted SRMs. On the other hand, the axial flux SRMs are divided into single-stack SRMs and multi-stack SRMs. In this subsection, the different configurations of the rotary SRMs are presented.

#### 1) RADIAL-FLUX ROTARY SRMs

Radial-flux rotary SRMs configurations comprise conventional long-flux-path, mutually coupled short-flux-path and PM-assisted SRMs. Conventionally, the flux flows through the entire stator back iron. In short-flux-path configurations, the flux flows in short loops containing the rotor and stator yokes and the adjacent poles [44]. The latter configuration has a relatively lower iron loss. However, it has higher mutual inductance between phases, which reduces the machine's fault tolerance capability [45]. Permanent Magnets (PMs) could be added to the stator in PM-assisted machines to increase the machine co-energy, which increases the torque density and efficiency [46], [47].

Radial-flux machines can have either an in-runner structure or out-runner structure, as shown in Fig. 2 and Fig. 3, respectively. The out-runner motors are more preferred for in-wheel drive applications as they can reduce the transmission losses significantly [27], [29], [48]–[50]. It also has higher torque density due to the extended lever arm, where the torque density may reach 2.4 times that of an in-runner counterpart for the same spatial constraints [51].

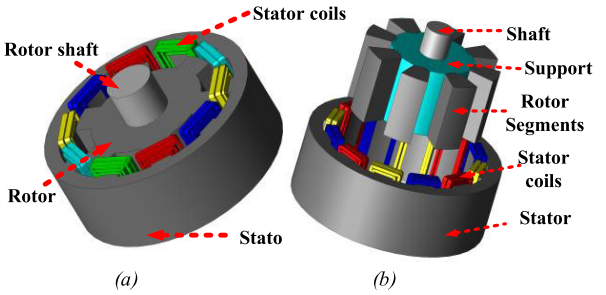


**FIGURE 2.** In-runner radial-flux SRMs; a) A five-phase 10/6 in-runner radial-flux SRM, and b) A three-phase 12/8 radial-flux segmented-rotor SRM [52].

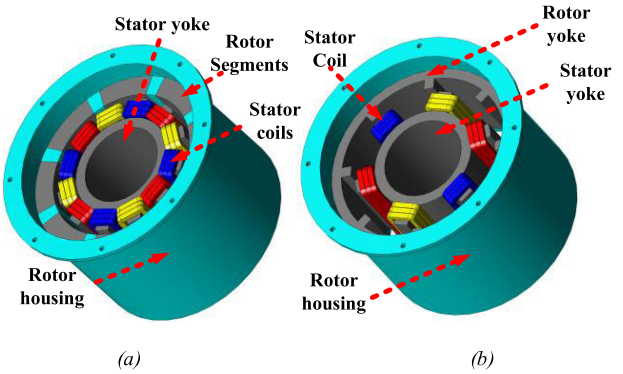


**FIGURE 3.** Out-runner radial-flux SRMs; a) short flux path 12/8 segmented-rotor SRM, and b) 6/8 non-segmented-rotor SRM.

The rotor can be non-segmented or segmented, as shown in Fig. 2 for in-runner configuration and Fig. 3 for out-runner configuration. The non-segmented design has a simple structure and provides higher average torque and lower torque ripple [49], [52]. On the other hand, the segmented design reduces the rotor weight and has higher torque density and lower rotor inertia [27]. The small rotor inertia also improves the machine's dynamic performance [27].

#### 2) AXIAL-FLUX SRMs

In axial-flux SRMs (AFSRMs), the flux travels axially between the stator and rotor. Due to the relatively shorter flux path, AFSRMs have a higher power density than radial-flux SRMs [30]. Based on the machine structure and number of stators and rotors used in the machine, AFSRMs can be classified into three main categories, as illustrated in Fig. 4. These categories include single-stator single-rotor (single-sided) machine, two-airgap (double-sided) machine, and multi-stack machine.

The single-sided type has the simplest structure as it consists of a single stator, a single rotor, and one airgap [31], [32]. A crucial problem of this configuration is the imbalance between the axial forces of the stator and rotor [33], [34], which produces high acoustic noise and

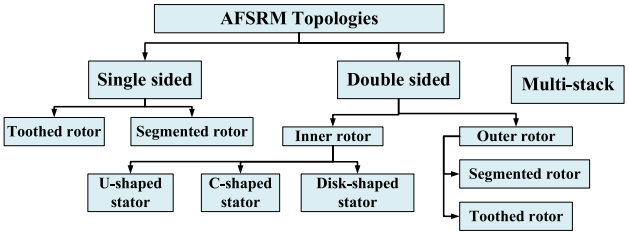


**FIGURE 4.** Main topologies of AFSRMs.

needs to be accommodated in the bearing design [18]. There are two types of single-sided AFSRMs: the toothed-rotor and segmented-rotor types, as shown in Fig. 5 and Fig. 6, respectively [30].

The toothed-rotor type stator consists of a yoke, teeth, and coils, whereas the rotor comprises a yoke and teeth. Alternatively, the stator of the segmented-rotor type consists of coil-wound teeth, auxiliary teeth, and a yoke [30]. The rotor consists of separate segments held together by a non-magnetic material such as aluminum or plastic. This SRM configuration has lower copper losses. It also has lower iron loss due to the auxiliary stator poles that provide a shorter flux path. Plastic or aluminum usage in the rotor to hold the rotor segments reduces the motor inertia, which improves the dynamic performance of the machine [53].

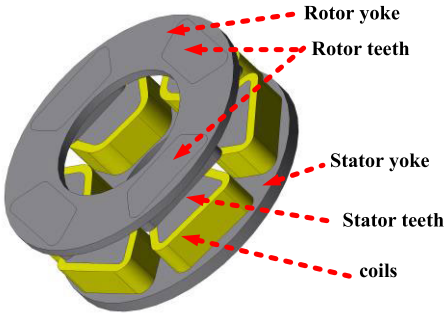


**FIGURE 5.** A single-sided toothed-rotor AFSRM.

Double-sided AFSRMs have a balanced axial force, and the available volume of this machine is more effectively used for torque production [35]–[37]. This configuration may have two outer rotors (dual-rotor configuration) or two outer stators (inner-rotor configuration). The dual-rotor configuration has either toothed [54] or segmented [55] rotors, as shown in Fig. 7 and Fig. 8, respectively. The segmented-rotor topology provides higher torque and efficiency than the toothed-rotor one [56]. The increase of the torque of the segmented-rotor type is due to the short flux path that provides higher flux linkage compared to the toothed-rotor type [56].

The dual-stator inner-rotor AFSRM, shown in Fig. 9, is typically utilized as an in-wheel actuator of electric vehicles [35], [57]. The rotor is segmented and sandwiched by two identical external stators [58]. This topology has a small axial length due to the absence of rotor yoke [57]. A non-magnetic carrier accommodates the rotor segments [59].

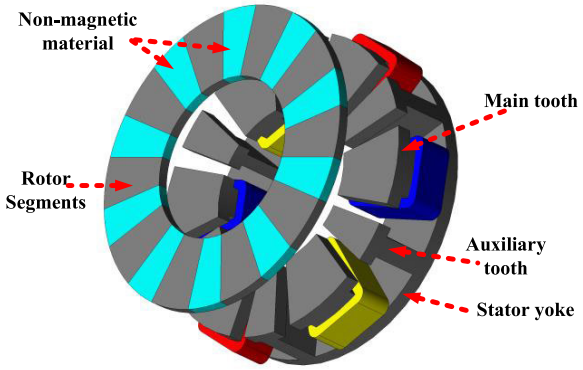


**FIGURE 6.** A single-sided segmented-rotor AFSRM.

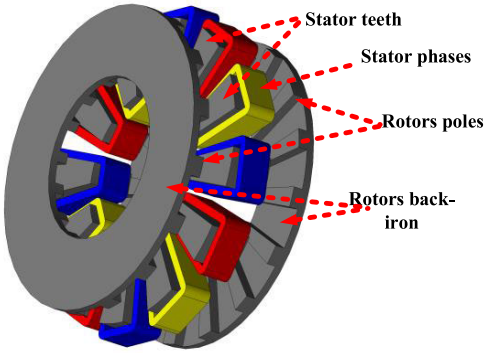


**FIGURE 7.** A 12/16 dual-rotor single-stator toothed-rotor AFSRM.

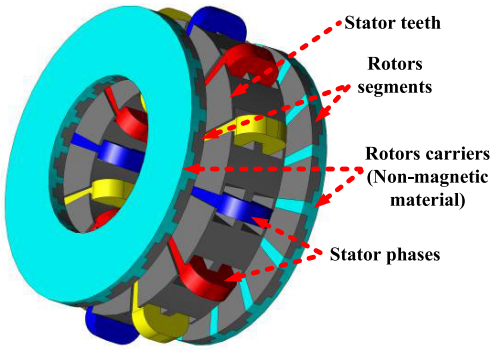


**FIGURE 8.** A 12/16 dual-rotor single-stator segmented-rotor AFSRM.

### B. LINEAR SRM

Linear SRMs (LSRMs) have a similar structure to rotary SRMs, except that the stator and rotor have a linear form. They consist of a stator (stationary part) and a translator (moving part) [38]. LSRMs configurations comprise planar and tubular configurations. Fig. 10 shows a three-phase unilateral-type planar LSRM with a four-pole translator.

The unilateral-type main disadvantage is the high unbalanced axial forces between the stator and the translator, causing immense friction between both parts. The friction potentially reduces the machine lifetime [39]. Bilateral-type (double-sided) LSRMs, with two equal airgaps, could solve this issue [40].

The tuber-type LSRM, shown in Fig. 11, consists of a tuber stator sleeve and a cylindrical translator [43]. A precise

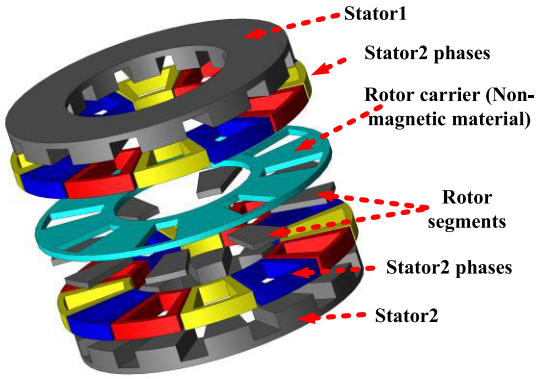


**FIGURE 9.** A 12/8 three-phase dual-stator inner-rotor axial-flux SRM.

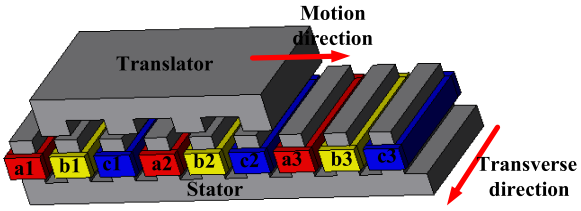


**FIGURE 10.** A three-phase unilateral-type planar LSRM with a four-pole translator.

shaft installation prevents unbalanced radial magnetic forces. Unlike unilateral- and bilateral-type LSRMs, the tuber-type LSRM does not have a transversal cut and has a uniform magnetic field distribution in the circumferential direction.

The tuber-type LSRM comprises transversal-flux [41]–[60], and longitudinal-flux [42] types according to the flux direction to the translator. Fig. 11 shows a double-excited-winding, where both stator and translator are excited, tubular longitudinal-flux LSRM [62].

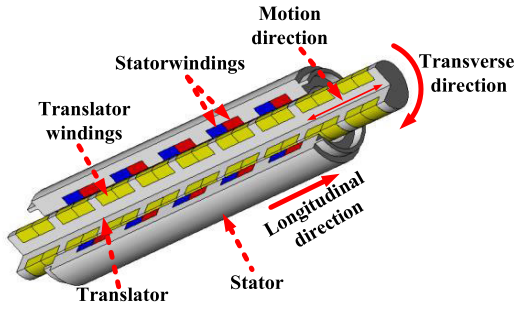


**FIGURE 11.** A double-excited-winding tubular longitudinal-flux LSRM [62].

## III. OBJECTIVE FUNCTIONS FOR PERFORMANCE IMPROVEMENT OF SRMs

This section reviews the different measures of the SRMs' performance, which are used as objective functions for performance improvement. These objectives include the maximization of torque, reduction of torque ripple, maximizing the efficiency, and mitigation of radial force for minimization of acoustic noise and vibration of the machine. In sections V and VI, more details about the use of these performance indices are presented.

### A. TORQUE RIPPLES

The SRM drives have more torque pulsation than other machine types due to the discrete nonlinear torque of each phase and the doubly salient structure of the machine. There are different definitions for torque ripples used in the literature as objective functions, for instance:

$$\Delta T = T_{\max} - T_{\min} \tag{1}$$

$$TR_n = \frac{T_{\max} - T_{\min}}{T_{av}} \tag{2}$$

$$TR_p = \frac{T_{\max} - T_{\min}}{T_{av}} \times 100\% \tag{3}$$

$$\Delta T_{rms} = \sqrt{\frac{1}{t_2 - t_1}\int_{t_1}^{t_2} (T(t) - T_{av})^2 dt}, \tag{4}$$

where $T_{\max}$ and $T_{\min}$ are the maximum and the minimum values of the torque profile over one electric cycle, $T_{av}$ is the average torque, and $T(t)$ is the instantaneous torque as a function of time. The duration $t_2 - t_1$ is the time of one complete electric cycle, $\Delta T$ is the peak-to-peak torque ripple, $TR_n$ and $TR_p$ are the normalized and percentage torque ripple respectively, and $\Delta T_{rms}$ is the RMS torque ripple. Fig. 12 shows the average torque and the peak-to-peak torque ripple in a typical torque waveform of 6/14 radial flux SRM over one electric cycle operating at 1500 rpm.

The peak-to-peak torque ripple, the normalized torque ripple, and the percentage torque ripple, shown in (1), (2), and (3) respectively, are simple, but only the maximum and the minimum values of the torque waveform are used to calculate the torque ripple. However, the RMS torque ripple expression, shown in (4), is a function of all the torque waveform data points and measures these points' deviation from the average torque line. The RMS torque ripple formula is often used for optimization to minimize the SRMs torque ripples and improve the machine torque quality [6].

Reducing the torque ripple of SRMs is one of the hot research topics. Geometry and topology optimization are common approaches to minimize the machine torque ripples. In literature, arc angles of rotor and stator poles, the height of rotor and stator poles, stator/rotor back iron thickness, number of phases, and stack length were used to minimize the machine torque ripple. Also, the material distribution inside the rotor and stator cores was optimized to reduce the torque ripple of SRMs [63], [64].

Moreover, drive control variables such as converter firing angle for each phase, conduction angle for each phase, reference current, and the current waveform shape were used for torque ripple minimization of SRMs. This research area is out of the paper scope, but the reader can find more in [6] and [65].

### B. AVERAGE TORQUE AND TORQUE DENSITY

PMSMs have the highest torque density among other machine types due to the permanent magnet excitation. For the SRMs, the average torque and the torque density can be enhanced through the selection of the rotor and stator core materials

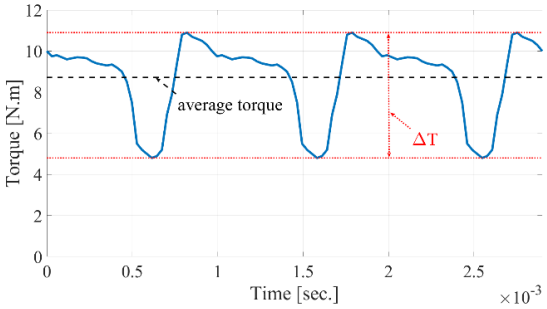


**FIGURE 12.** Typical torque waveform over one electric cycle of 6/14 SRM at 1500 rpm speed.

and optimizing the machine structure through geometry or topology optimization [66]. The cobalt iron and 6.5% silicon iron are usually used in SRMs to increase the torque density due to the higher saturation limit that boosts the machine's magnetic loading [66], [67].

Fig. 12 shows the average torque (black dotted line) of a 6/14 SRM torque profile operating at 1500 rpm speed. The average torque can be calculated using the following equation over one complete electric cycle:

$$T_{av} = \frac{1}{t_2 - t_1} \int_{t_1}^{t_2} T(t)dt, \tag{5}$$

The torque density (in N.m/L) of the motor is defined as the motor average torque to the motor volume. Also, the specific torque (in N.m/kg) can be used as an optimization function which is the ratio between the average torque and the motor weight. Geometry and topology optimizations of SRMs were extensively applied in the literature to enhance the average torque and torque density.

### C. EFFICIENCY IMPROVEMENT

The SRM efficiency is commonly used as an objective function in literature to improve machine performance. The core losses ($P_{core}$), the rotor windage loss ($P_{win}$), and the copper losses ($P_{cu}$) are the primary loss sources in SRMs. Minimizing these losses can improve the SRMs efficiency, as illustrated in the following equation:

$$\eta = \frac{P_{mech}}{P_{elec}} = \frac{P_{mech}}{P_{mech} + P_{cu} + P_{core} + P_{win} + P_{other}}, \tag{6}$$

where $\eta$ is the SRM efficiency, $P_{mech}$ is the output mechanical power, $P_{elec}$ is the input electrical power, and $P_{other}$ is the other losses that are not related to the electromagnetic design as the bearing friction loss. The rotor windage loss is included as an electromagnetically dependent parameter in this equation since it depends on the rotor design due to the salient nature of the rotor structure.

The selection of the machine material can improve the machine's efficiency. Copper magnet wires are usually used for the coils due to the high thermal conductivity, high current carrying capacity, and low electric resistivity compared to Aluminum counterparts [6]. The core loss can be reduced by using low-loss magnetic steel, such as 6.5% high silicon steel, low-loss silicon steel, laminated amorphous alloy, high-resistivity soft magnetic composites [68]–[70]. In addition to the materials' selection, the SRMs key design parameters and the material distribution in the design space are optimized to improve the machine efficiency. This will be discussed in more detail in sections V and VI.

### D. RADIAL FORCE AND ACOUSTIC NOISE

The high radial force components of SRMs are considered one of the big challenges. Radial forces are the main sources of SRM vibration and acoustic noise [6], [71]. As mentioned in [71], the acoustic noise radiated from SRMs is relatively harsher compared to induction machines and PMSMs, which limits utilizing the SRMs in noise- and vibration-sensitive applications like white goods [71]. Consequently, analyzing and reducing SRMs acoustic noise receives much attention between researchers [72]–[74].

In SRMs and electric machines in general, there are three primary sources of acoustic noise and vibration: mechanical sources, aerodynamic sources, and electromagnetic sources. In this paper, the review is focused on the electromagnetic source of acoustic noise. The electromagnetic cause of acoustic noise and vibration of SRMs is related to the machine excitation, which generates radial pressure on the machine structure that can excite its natural frequency at different mode shapes [75]. Fig. 13 shows a typical radial pressure on the stator structure of three-phase inner rotor 6/4 SRM for one electric cycle. The radial force shown in the figure represents the magnetic attraction between stator teeth and rotor teeth in the radial direction, which deforms the machine stator structure. This deformation appears in different mode shapes [76]. The radial force density acting on the machine's different structures can be decomposed into different axial, circumferential, and temporal harmonic orders $(ax, \upsilon, u)$. In some cases, only the first axial mode is considered $(ax = 1)$, and the force density is decomposed to $(\upsilon, u)$ harmonic orders. The forcing frequency of each of these harmonics depends on the harmonic temporal order and the mechanical frequency and can be calculated as follows:

$$f_f(u) = |u| N_r f_{mech} = |u| N_r \frac{n}{60} [Hz], \tag{7}$$

where $f_f$ is the forcing frequency of a radial force harmonic with electric temporal order $u$, $f_{mech}$ is the rotor mechanical frequency, $N_r$ is the number of rotor poles, and $n$ is the rotor speed in rpm. Fig. 14 shows the 2-D FFT of the radial pressure acting on the stator structure that is illustrated in Fig. 13 as an example of the radial pressure harmonic spectrum.

Generally, the stator vibration in radial-flux SRMs is modelled as the vibration of an equivalent cylindrical shell. The vibration modes of SRMs stator are identified in circumferential and axial directions. Fig. 15 shows examples of different circumferential mode shapes of a cylindrical shell. Each of these modes has a natural frequency depending on the structure dimensions and material properties, such as Young's modulus and Poisson's ratio. The radial force density

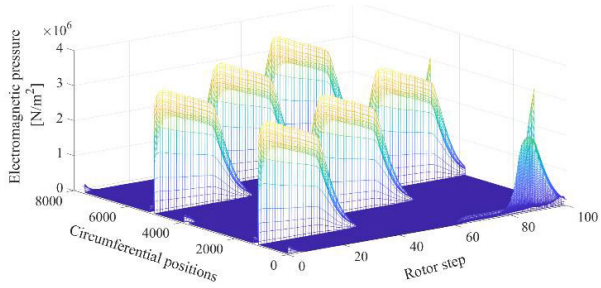


**FIGURE 13.** A typical radial force density acting on the stator of 6/4 SRM operating at 1103 rpm, and the rotor rotates at the counterclockwise direction.

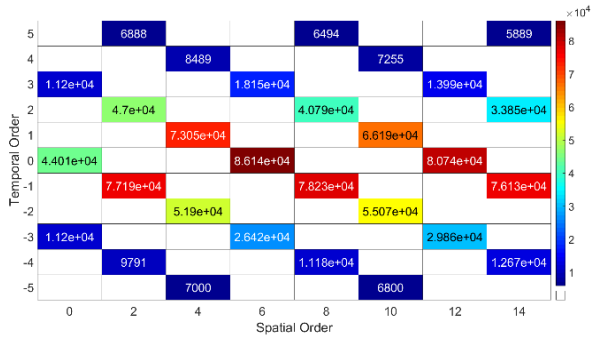


**FIGURE 14.** 2-D FFT of the radial force density wave shown in Figure 13 (the temporal order shown in this figure is the electrical temporal order).

harmonics excite the stator structure, and the acoustic noise occurs when the forcing frequency of a certain spatial harmonic order becomes close to the natural frequency of the corresponding circumferential mode shape.

Fig. 16 shows the intersection between the natural frequency of six circumferential mode shapes of a stator structure ($Circ = \{0, 2, 4, 6, 8, 10\}$) with the forcing frequency of five temporal order ($u = \{1, 2, 3, 4, 5\}$) of an inner rotor 6/4 SRMs. In the figure, the rays represent the change of the harmonic pressure frequency with rotor speed. It can be concluded from Fig. 14 and Fig. 16 that the motor at the base speed will excite the circumferential mode shapes $Circ = \{2\}$ with the harmonics $(\upsilon, u) = \{(2, -1)\}$, $Circ = \{4\}$ with the harmonics $(\upsilon, u) = \{(4, -2)\}$, and $Circ = \{6\}$ with the harmonics $(\upsilon, u) = \{(6, -3), (6, 3)\}$. The acoustic noise can be mitigated by either reducing the amplitude of these dominant harmonics or making the machine structure stiffer. A stiffer structure has a higher natural frequency of the different mode shapes, making it difficult to be excited within the motor speed range.

The geometrical design parameters of SRMs can be optimized to minimize the amplitude of the most dominant harmonics that contribute to the acoustic noise [77]. The natural frequency of the different circumferential mode shapes of the machine structure can be controlled by the mechanical design and the used materials as illustrated in [72], which can be used to mitigate the acoustic noise as illustrated in [78]. The drive control variables such as the phase firing angle, the turn-off-angle, the reference current, and the current profile were used in the literature to eliminate or reduce the amplitude of selective spatial harmonic orders to minimize the acoustic noise as discussed in [79]–[82].

## IV. OPTIMIZATION METHODS

Several optimization methods have been applied to the design of SRMs. These optimization methods are generally divided into deterministic and stochastic optimization techniques. Deterministic optimization techniques require gradient information, whereas stochastic optimization techniques search for an optimal solution in a randomized way that does not require the objective function's gradient information. Deterministic optimization techniques reach an optimal solution faster and provide a unique and precise solution [83]. However, the achieved solution is not guaranteed to be the global optimal solution for nonconvex functions [83]. The machine design is usually a nonconvex problem with many local solutions. This makes it challenging for deterministic optimization techniques to reach a global solution. The optimization process can also be divided based on the number of objective functions to single-objective optimization and multi-objective optimization.

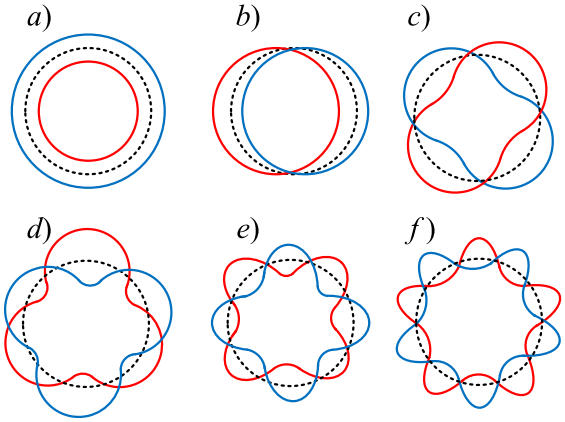


**FIGURE 15.** Circumferential vibration modes of radial-flux SRMs stator. a) Mode 0, b) Mode 1, c) Mode 2, d) Mode 3, e) Mode 4, f) Mode 5.

This section reviews some of the deterministic and stochastic optimization techniques used in electrical machine design. The deterministic optimization techniques and the different ways to obtain the objective function gradient with respect to the design parameters are discussed first. Then, the stochastic optimization techniques are reviewed. At the end of this section, the multi-objective optimization problem is discussed, and the multi-objective optimization techniques used for SRMs design are reviewed.

### A. DETERMINISTIC OPTIMIZATION METHODS

Deterministic optimization methods use objective function gradients with respect to the design parameters to guide the optimization iterates to the optimal solution [84]. The convergence of a gradient-based optimizer depends on the accuracy of the obtained gradients [85].

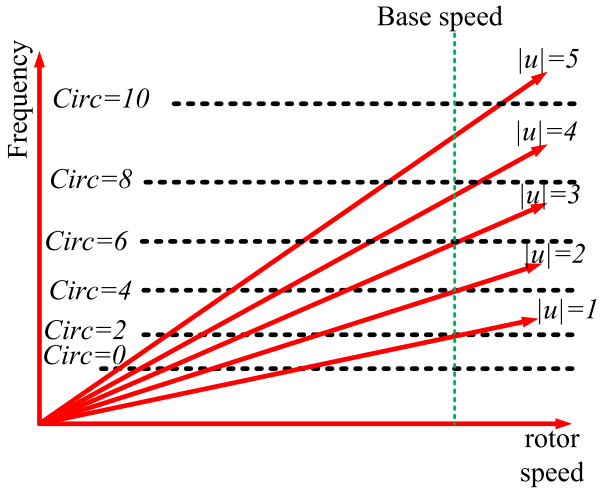


**FIGURE 16.** An illustration of the forcing frequency versus rotor speed and the excitation of different circumferential vibration modes of a 6/4 SRM.

In this subsection, the objective function gradient estimation methods are covered first. Then, the deterministic optimization algorithms used for SRMs are reviewed.

### 1) OBJECTIVE GRADIENT CALCULATION METHODS

The gradients (the objective function sensitivity to the design parameters) can be estimated through numerical methods, adjoint variable methods, or using automatic differentiation, as categorized in Fig. 17. Gradients are routinely computed numerically using forward finite difference (FFD) [86], backward finite difference (BFD) [86], central finite differences (CFD) [87]–[89], and complex-step methods [89]. The FFD and BFD methods require one additional simulation for each design parameter, whereas the more accurate CFD requires two extra simulations for each design parameter. This means that the FFD and BFD require $n+1$ simulations, whereas the CFD requires $2n+1$ simulations for each iteration, where $n$ is the number of the design parameters.

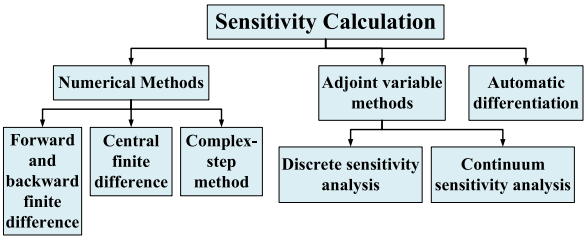


**FIGURE 17.** Methods of Sensitivity calculation.

The approximations of these three methods when calculating the gradient of the objective function f with respect to x at xi are illustrated in Fig. 18. A perturbation h is utilized in this figure. All three methods are computationally expensive and may require a convergence study to define the appropriate perturbation size $h$ [89]. On the other hand, the obtained gradients using the complex-step method (CSM) are more accurate than those obtained with finite difference methods [85]. The CSM is not subject to roundoff errors, and it can be generalized to any objective function [90]. However, it deals with a complex number variables, which is not applicable to the SRMs design as all the parameters are real.

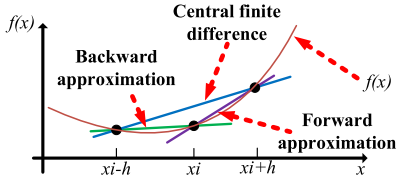


**FIGURE 18.** A clarification of the finite difference methods.

The discrete adjoint variable method [91]–[93] and continuum adjoint variable method [94]–[97] outperform the finite difference methods in the number of required objective function evaluations at each step [85]. Unlike finite difference methods, they obtain the objective function gradient with respect to all design parameters using one additional simulation for each iteration [88], [91], [98].

The discrete approach is typical as its equations are applicable to almost all FEA-based problems. However, the sensitivity calculation requires information like the FE system matrix and vector, which are not usually accessible. This limitation has been solved in [77] as the authors were able to use the available data to reconstruct the FE system matrix and vector and use it for discrete adjoint variable sensitivity calculation of SRM radial force with respect to the different design parameters.

On the other hand, the continuum approach does not require extensive access to the FE internal data structures. This method obtains sensitivity by differentiating the governing variational equation before discretization. The sensitivity formulas are formed using the material derivative concept of the continuum mechanics and based on the analytical equations of the state and the adjoint variables as described in [94] and [95].

Lastly, the automatic differentiation (AD) method calculates the derivatives of a computer program output with respect to the inputs. It repeatedly applies the chain rule to the program sequence of elementary arithmetic operations and functions. The AD method has two operating modes, namely forward accumulation and reverse accumulation [99]. The two modes compute the gradient of the function with a seed vector that has the same number of the function inputs or outputs for forward accumulation and reverse accumulation, respectively [99]. The AD method was used to find the sensitivity of the electromagnetic force to different geometric parameters of a linear actuator in [100].

The optimal solutions determined by deterministic optimization methods are based on the accuracy of gradient calculations. There is a trade-off between the method accuracy and optimization time, so the most suitable method to be used depends mainly on the application and project timeline.

### 2) DETERMINISTIC OPTIMIZATION ALGORITHMS USED FOR SRMs

Deterministic optimization methods usually utilize a single-objective function. Multiple objectives can be weighted together using aggregation methods such as arithmetic mean operator, harmonic mean operator, and Bonferroni mean [101]. Deterministic optimization methods can also be classified as unconstrained and constrained methods. The constrained methods are considered here since there are usually spatial constraints on the different design parameters of SRMs and electric machines design in general [102].

There are many constrained optimization methods that were applied to electric machines design. These include sequential quadratic programming, Lagrangian method, and interior point method, as shown in Fig. 19 [83].

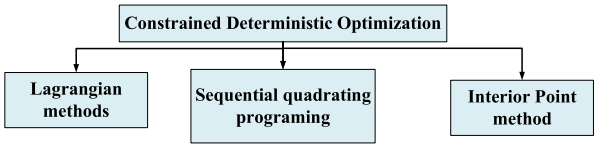


**FIGURE 19. Methods of constrained deterministic optimization [83].**

A general optimization problem (given in (8), (9), and (10)) is used to describe and illustrate the different deterministic optimization methods throughout this section.

$$\text{minimize: } f(\boldsymbol{x}) \tag{8}$$

$$\text{Subject to: } g_i(\boldsymbol{x}) \leq 0, \quad i = 1, 2, \ldots m, \tag{9}$$

$$\text{Subject to: } h_j(\boldsymbol{x}) = 0, \quad j = 1, 2, \ldots l, \tag{10}$$

where $f(\boldsymbol{x})$ is the objective function, $\boldsymbol{x}$ is the vector of the design variables, The design space is also subject to $m$ numbers of inequality constraints and $l$ numbers of equality constraints as described in (9) and (10), respectively. The upper and the lower values of the design variables are considered here a part of the inequality constraints in (9). We consider in what follows some of the key optimization methods used in the optimization problem solution given by (8)-(10).

### 3) LAGRANGIAN METHOD

The Lagrangian method [84] creates and solves a subproblem obtained by linearizing the constraints and applying Lagrange function approximation at each step. In the algorithm, the objective function and all the equality and inequality constraints are combined in a single function as shown in (11). $m$ slack variables, $\boldsymbol{y} = [y_1, y_2, \ldots, y_m]$, are added to the inequality constraints to create the Lagrange function:

$$(\boldsymbol{x}, \boldsymbol{y}, \boldsymbol{\lambda}, \boldsymbol{\mu}) = f(\boldsymbol{x}) + \sum_{i=1}^{m} \lambda_i \left(g_i(\boldsymbol{x}) + y_i^2\right) + \sum_{j=1}^{l} \mu_j \left(h_j(\boldsymbol{x})\right), \tag{11}$$

where $\boldsymbol{\lambda} = [\lambda_1, \lambda_2, \ldots, \lambda_m]$ are the Lagrange multipliers for the inequality constraints and $\boldsymbol{\mu} = [\mu_1, \mu_2, \ldots, \mu_l]$ are the Lagrange multipliers for the equality constraints. The problem described in (11) has $(n + 2m + l)$ unknown variables, where $n$ is the number of the design variables. A system of equations can be formed to solve all of these unknowns by forming the gradient of the Lagrange function with respect to all unknowns, as illustrated in [84].

The sequential quadratic programming, NLPQLP, and the interior point methods are based on the Lagrangian function to solve the optimization problem.

### 4) SEQUENTIAL QUADRATIC PROGRAMMING (SQP)

This is an iterative method that uses the objective function's gradient for nonlinearly constrained problems [103]. This method is considered one of the most effective methods for solving constrained nonlinear optimization problems. The method solves subproblems in which the cost function is approximated as a quadratic function with linearized constraints [83]. The SQP is a time-efficient method if the number of design parameters is not too large, the objective function and its gradients can be obtained with high accuracy, the problem is smooth, and the design parameters are well-scaled [104].

The basic idea of this method is to form a quadratic programming subproblem at each step based on a quadratic approximation of the Lagrange function, (11). Then the quadratic programming can be formed as follows:

$$\min_{\boldsymbol{d}} \ \nabla f(\boldsymbol{x}^k)^T \boldsymbol{d} + \frac{1}{2} \boldsymbol{d}^T \boldsymbol{H}^k \boldsymbol{d}, \tag{12}$$

$$\text{Subject to: } \nabla g_i(\boldsymbol{x}^k)^{\mathrm{T}} \boldsymbol{d} + g_i(\boldsymbol{x}^k) \leq 0, \quad i = 1, 2, \ldots m. \tag{13}$$

$$\text{Subject to: } \nabla h_i(\boldsymbol{x}^k)^{\mathrm{T}} \boldsymbol{d} + h_i(\boldsymbol{x}^k) = 0, \quad i = m + 1, \ldots m + l., \tag{14}$$

where $\boldsymbol{d}$ is the search direction of the design parameters, $\nabla f(\boldsymbol{x}^k)$ and $\boldsymbol{H}^k$ are the objective function gradient and the Hessian matrix of the Lagrangian function at iteration number $k$, respectively, and $\nabla g_i(\boldsymbol{x}^k)$ and $\nabla h_i(\boldsymbol{x}^k)$ are the gradient of the inequality and equality constraints at iteration number $k$, respectively.

At each iteration, the Hessian matrix of the Lagrange function is approximated. The Hessian matrix can be approximated by the Broydon Fletcher Goldfarbo Shanno (BFGS) approximation as follows [105]:

$$\boldsymbol{H}^{k+1} = \boldsymbol{H}^k + \frac{\left[\boldsymbol{V}^k\right]^T \boldsymbol{V}^k}{\left[\boldsymbol{V}^k\right]^T \boldsymbol{U}^k} - \frac{\boldsymbol{H}^k \boldsymbol{U}^k \left[\boldsymbol{U}^k\right]^T \left[\boldsymbol{H}^k\right]^T}{\left[\boldsymbol{U}^k\right]^T \boldsymbol{H}^k \boldsymbol{U}^k}, \tag{15}$$

$$\boldsymbol{V}^k = \nabla \boldsymbol{L}^{k+1} - \nabla \boldsymbol{L}^k, \tag{16}$$

$$\boldsymbol{U}^k = \boldsymbol{x}^{k+1} - \boldsymbol{x}^k, \tag{17}$$

where $\nabla \boldsymbol{L}$ is the gradient of the Lagrange function.

After solving the quadratic programming subproblem for the search direction $\boldsymbol{d}$, a linear search algorithm can be used to minimize the objective function along the search direction and update the variable vector as follows:

$$\boldsymbol{x}^{k+1} = \boldsymbol{x}^k + \alpha \boldsymbol{d}, \tag{18}$$

where $\alpha$ is the optimal change of the design variable.

After determining the new design variable, the process is repeated till it reaches the termination conditions. Fig. 20 shows a flowchart of the sequential quadratic programming method.

The SQP is considered one of the powerful deterministic optimization techniques. The only problem related to this technique is the high computational cost for each optimization step [106].

#### 5) INTERIOR-POINT METHOD

The interior-point method (IPM) is a constrained optimization method used for SRMs and electrical machines design optimization. The IPM is a linear optimization technique based on the logarithmic barrier method to solve the linear and nonlinear optimization problem as discussed in [107].

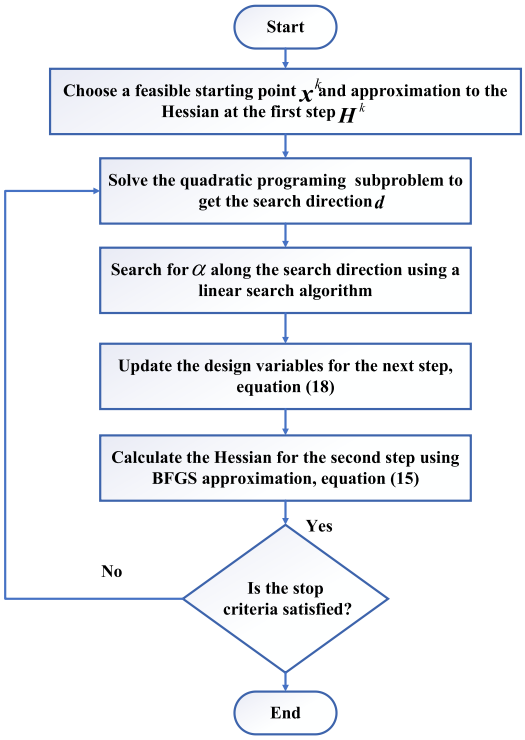


**FIGURE 20.** A flow chart of the sequential quadratic programming algorithm.

By using a barrier function in IPM, consider a nonlinear optimization problem such as in (8) and (9), the constrained optimization problem is transformed into an unconstrained optimization problem as follows [108]:

$$R(\boldsymbol{x}, \mu) = f(\boldsymbol{x}) - \mu \sum_{i=1}^{m} \log(g_i(\boldsymbol{x})) \tag{19}$$

where $\mu$ is a positive scalar variable and called the barrier coefficient. As $\mu$ converges to zero, the minimum of (19) converges to the solution of (8). The gradient of the barrier function given in (19) is given as follows:

$$\nabla R = \nabla f(\boldsymbol{x}) - \mu \sum_{i=1}^{m} \frac{1}{g_i(\boldsymbol{x})} \nabla g_i(\boldsymbol{x}) \tag{20}$$

In addition to the function variable $\boldsymbol{x}$, the Lagrange multiplier $\boldsymbol{\lambda}$ is introduced as follows:

$$g_i(\boldsymbol{x})\lambda_i = \mu, \quad \forall_i = 1, \ldots., m. \tag{21}$$

From (20) and (21), the gradient of the barrier function becomes:

$$\nabla f(\boldsymbol{x}) - \boldsymbol{A}^T \boldsymbol{\lambda} = 0, \tag{22}$$

where $\boldsymbol{A}$ is the Jacobian vector of the constraints. The Newton's method is then applied to (21) and (22) as follows:

$$\begin{pmatrix} \boldsymbol{H} & -\boldsymbol{A}^T \\ \boldsymbol{\Lambda A} & \boldsymbol{G} \end{pmatrix} \begin{pmatrix} \boldsymbol{S}_x \\ \boldsymbol{S}_\lambda \end{pmatrix} = \begin{pmatrix} -\nabla f(\boldsymbol{x}) + \boldsymbol{A}^T \boldsymbol{\lambda} \\ \mu - \boldsymbol{G\lambda} \end{pmatrix} \tag{23}$$

where $\boldsymbol{H}$ is the Hessian matrix of the barrier function, (19), $\boldsymbol{G}$ is a diagonal matrix with $G_{ii} = g_i(\boldsymbol{x})$. The system of equations in (23) is solved for the design variable search direction, and the Lagrange coefficients search direction, then the design variables and the Lagrange coefficients are updated for the next step as follows:

$$\begin{aligned} \boldsymbol{x}^{k+1} &= \boldsymbol{x}^k + \alpha \boldsymbol{S}_x \\ \boldsymbol{\lambda}^{k+1} &= \boldsymbol{\lambda}^k + \alpha \boldsymbol{S}_\lambda \end{aligned} \tag{24}$$

The best value of $\alpha$ can be found by the linear search along the search direction of the design variables and the Lagrange coefficients. The Hessian matrix in (23) can be estimated for the next step by the BFGS approximation, as illustrated in (15). The algorithm keeps iterating till the termination condition of the algorithm occurs [109].

In summary, this subsection reviewed the deterministic optimization technique used in the literature for electric machine design. The reader can find a detailed review of the various constrained deterministic optimization methods in terms of simplicity, reliability, and efficiency in [83].

### B. STOCHASTIC OPTIMIZATION METHODS

Stochastic optimization techniques search for an optimal solution with randomness. They can deal with either single-objective or multi-objective optimization problems. Different stochastic algorithms considered in this review include:

1) Swarm Optimization (SO) [110]–[113]: The algorithm mimics natural creatures' social behavior, such as birds and wolves, in searching for food.
2) Simulated Annealing (SA) [114], [115]: The algorithm simulates the heat treatment annealing process to reach the best value of the design objectives.
3) Genetic Algorithm (GA) [116]: The algorithm imitates the evolution process of species.
4) Evolutionary Algorithms (EAs) [117]: These algorithms mimic the evolution process of species based on the concept of natural selection. GA can be considered as a subdivision of the EAs. The main difference is that the parent selection in EAs is based on an equal probability of each individual, whereas the parent selection in GA is based on the likelihood of success and the parents' fitness values.

### 1) SWARM OPTIMIZATION TECHNIQUES

Many optimization techniques are inspired by the social behavior of creatures in searching for food such as particle swarm optimization [110], [111], ant colony [118], artificial bee colony [119]–[121], glowworm [122], [123], firefly [124], [125], cuckoo search [126], bat search [127], and hunting search [128]. The swarm optimization algorithms are simple, robust, and do not require the implementation of complex mathematical formulations [129].

Particle swarm optimization (PSO) was introduced by Kennedy and Eberhart more than 25 years ago [110]. It is a heuristic optimization technique that mimics the social behaviour of a group of creatures that search for food and follow the group's leader. A flowchart that describes the particle swarm optimization algorithm is shown in Fig. 21. In PSO, each particle (individual) location is a point in the design space. Each individual particle of the swarm is shifted at each iteration with a velocity that is a function of the best-achieved self and global locations at the current iteration. This is represented mathematically as given in (25) and (26).

$$\boldsymbol{x}_i^k = \boldsymbol{x}_i^{k-1} + \boldsymbol{V}_i^k \tag{25}$$

$$\boldsymbol{V}_i^k = w\boldsymbol{V}_i^{k-1} + C_1 d_1(\bar{\boldsymbol{x}}_i - \boldsymbol{x}_i^{k-1}) + C_2 d_2(\tilde{\boldsymbol{x}} - \boldsymbol{x}_i^{k-1}) \tag{26}$$

where $\boldsymbol{x}_i^k$ and $\boldsymbol{V}_i^k$ are the position and the velocity of the $i^{th}$ particle at the $k^{th}$ iteration, respectively, $\bar{\boldsymbol{x}}_i$ is the best local solution of the $i^{th}$ particle, and $\tilde{\boldsymbol{x}}$ is the best global solution of all particles. $C_1$ represents the cognitive learning factor that connects each particle to its own best value. The best global value is connected to each particle through the cognitive learning factor $C_2$. $w$ is an acceleration factor that should be high at the first few iterations to explore a larger area in the parameters space. It then gets smaller to make the algorithm converge faster. $d_1$ and $d_2$ take random values between 0 and 1.

As shown in Fig. 21, the algorithm starts by evaluating a random population's fitness with random positions and velocities. Then, the local minimum of that population is stored and compared to that of the next population. The algorithm updates the velocity and the positions of all population particles based on (25) and (26). The algorithm keeps running till the termination conditions are satisfied.

### 2) SIMULATED ANNEALING OPTIMIZATION

Simulated annealing algorithm is one of the stochastic optimization methods used extensively in the literature in electrical machines design optimization [64], [115], [130]. The algorithm is based on the heat treatment process of steel. It starts from a condition where the steel particles have high energy and in high instability and motion conditions. The particles cool down and reach a thermal equilibrium where they are arranged in a structure with lower internal energy through the optimization process. Through this process, the temperatures of the particles gradually decrease, and the objective function tends to reach the optimal solution. Fig. 22 illustrates a typical procedure of the simulated annealing optimization technique. The algorithm starts from an initial feasible point $\boldsymbol{x}^k$ in the design space where the objective function $f(\boldsymbol{x}^k)$ is evaluated. The equivalent temperature $T_k$ at the $k^{th}$ iteration is estimated based on (27).

$$T_k = T_{k-1}\left(1 - \frac{k-1}{k_{\max}-1}\right)^p \tag{27}$$

where $T_{k-1}$ and $k_{\max}$ are the temperature of the previous step and the maximum number of allowable iterations, respectively, with the annealing coefficient $p > 1$. This is not the only cooling formula used in simulated annealing optimization algorithm and the reader can find other cooling formulas in [83].

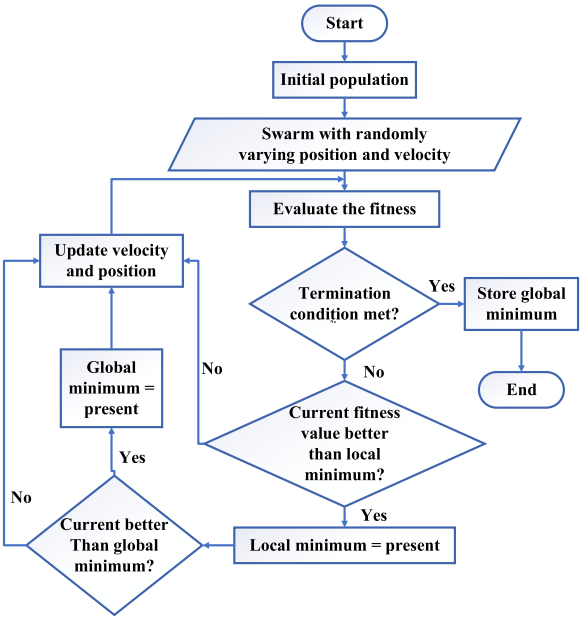


**FIGURE 21.** A flowchart of the particle swarm optimization algorithm.

The Metropolis rule is a step to accept the solution with a probability, $y$, based on the new particle energy, $E(\boldsymbol{x}_{new})$, and the old particle energy $E(\boldsymbol{x}_{old})$ as follows [131]:

$$y = \begin{cases} 1 & \text{if } E(\boldsymbol{x}_{new}) < E(\boldsymbol{x}_{old}) \\ \exp\left(-\dfrac{E(\boldsymbol{x}_{new}) - E(\boldsymbol{x}_{old})}{T}\right) & \text{if } E(\boldsymbol{x}_{new}) \geq E(\boldsymbol{x}_{old}) \end{cases} \tag{28}$$

Based on the algorithm flowchart in Fig. 22, the Metropolis algorithm is a very important step in the SA algorithm to find the optimal solution of the problem.

In [130], a general multi-objective SA algorithm was utilized in a machine-related optimization process. The algorithm was compared to the classical PSO, attraction-repulsion-based PSO, Gaussian mutation-based PSO, and quadratic interpolation-based PSO. The SA algorithm outperformed all these algorithms in terms of accuracy, robustness, stability, and convergence rate.

The SA algorithm could improve the performance of classical PSO. Classical PSO does not have an effective global

search, so it may not converge to the global solution and converge instead to a local one [132]. SA can enhance PSO robustness and effectiveness through the discrete PSO-SA algorithm at the expense of longer convergence time since more computations are required [132].

### 3) GENETIC ALGORITHM OPTIMIZATION

The genetic algorithm (GA) was first introduced in the 1960s [83]. It mimics the evolution process of the species and the concept of natural selection. This is mainly performed through the processes of parents' selection, crossover, and mutation, as illustrated in Fig. 23. The parents (parameters values) are selected first based on their fitness value (objective function value). The selection is generally based on a probability function that uses high-fitness individuals to produce offspring from their chromosomes. This means that the community fittest elements have the highest chance to produce the next generation. The algorithm encodes the values of the parents into binary strings. All the variables' binary strings are connected to a chromosome. As shown in Fig. 23, the parents' strings, blue and red, breed through the crossover process where the parents share their chromosomes to generate children. A random bit in each child string is then selected and inverted through the mutation process.

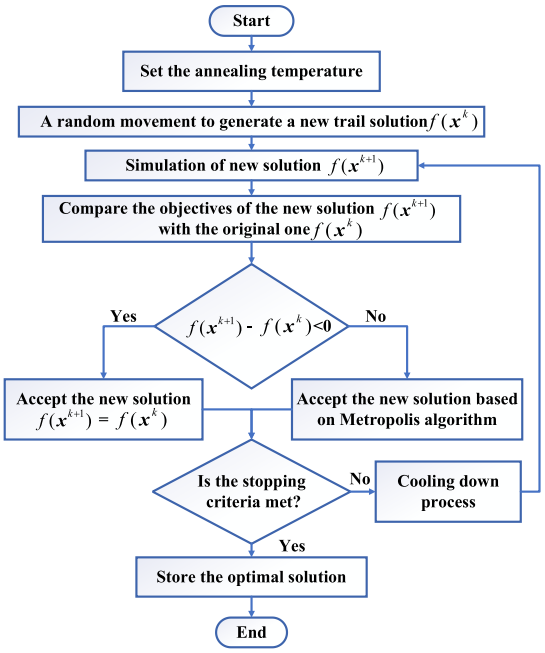


**FIGURE 22.** A flowchart of the simulated annealing optimization algorithm.

Fig. 24 shows a flow chart of the GA procedure [133]. The algorithm begins with an initial population with $m$ number of individuals. The fitness of each of these design points (individuals) is calculated. In the $k^{th}$ generation, two individuals are chosen as two parents. The crossover process is then applied with a high probability of up to 0.9 to all the individuals with high fitness. Two children are created when the crossover happens. The crossover probability, $r_c$,

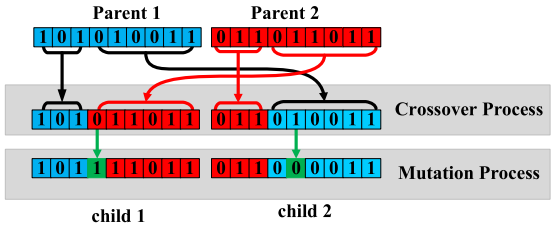


**FIGURE 23.** The crossover and mutation processes of the GA optimization technique.

controls the exploitation of the high fitness individuals to generate offsprings. In contrast, if there is no crossover, the two children will be copies of their parents. The mutation is then applied with a minimal probability of up to 0.01 to each of the two children. The mutation probability, $r_m$, controls the exploration process and prevents the early convergence to a local optimum solution. The new population replaces the old one, and the fitness of the $m^{th}$ population individual is evaluated. The crossover and the mutation processes are repeated until the termination condition is reached [133].

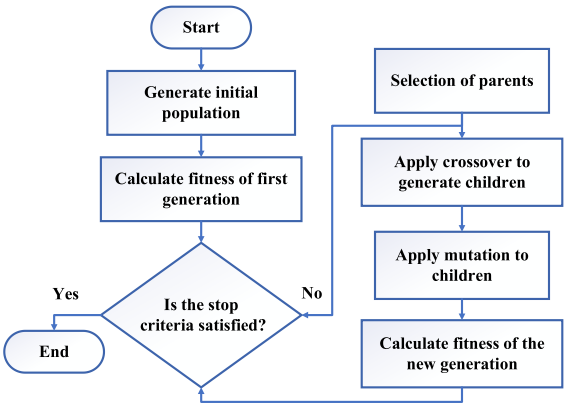


**FIGURE 24.** A flowchart of GA optimization.

The formulation of the population for a new generation in the GA is directly influenced by $r_c$ and $r_m$. In [134], the author showed that the fixed values of these two parameters are less effective than the adapted values, and a better improvement in the problem of global optimal point convergence can be achieved if these two parameters become adaptive and dynamic. A fuzzy inference system was proposed in [135] to adapt the values of $r_c$ and $r_m$ which improve the GA performance. This algorithm is called genetic fuzzy algorithm (GFA) and is used in SRMs design in the literature [136].

In order to deal with the nonlinear constraint, an augmented Lagrangian genetic algorithm (ALGA) is proposed in [137]. The optimization problem solved by ALGA is defined as follows:

$$\text{minimize: } f(\boldsymbol{x}) \tag{29}$$

$$\text{Subject to: } g_i(\boldsymbol{x}) \leq 0, \quad i = 1, 2, \ldots m, \tag{30}$$

$$\text{and } h_j(\boldsymbol{x}) = 0, \quad j = 1, 2, \ldots l, \tag{31}$$

$$\text{and } \boldsymbol{A}\boldsymbol{x} \leq \boldsymbol{B}, \tag{32}$$

$$\text{and } \boldsymbol{x}_{lb} \leq \boldsymbol{x} \leq \boldsymbol{x}_{ub}, \tag{33}$$

where $\boldsymbol{x}_{lb}$ and $\boldsymbol{x}_{ub}$ are the lower and upper limits of the design, respectively. The constraints in this method are divided into two types: the nonlinear constraints, (30) and (31), and linear constraints, (32) and (33). A subproblem is formulated by combining the nonlinear equality and inequality constraints with the objective functions using the Lagrangian and the penalty functions as follows:

$$R(\boldsymbol{x}, \boldsymbol{\lambda}, \boldsymbol{s}, \rho) = f(\boldsymbol{x}) - \sum_{i=1}^{m} \lambda_i s_i \log(s_i - g_i) + \sum_{j=1}^{l} \lambda_{(j+m)} h_j + \frac{\rho}{2} \sum_{j=1}^{n} h_j^2, \quad (34)$$

where $\boldsymbol{\lambda}$ is the Lagrangian multiplier estimate, $\boldsymbol{s}$ is a nonnegative shift, and $\rho$ is a penalty parameter. The algorithm starts with an initial value of $\rho$. The GA algorithm minimizes a series of subproblems. At each one of the subproblems $\boldsymbol{\lambda}, \boldsymbol{s}$ and $\rho$ are constants. When the subproblem is minimized with the required accuracy, the values of $\boldsymbol{\lambda}, \boldsymbol{s}$ and $\rho$ are updated to form the next subproblem. This process is repeated till reaching the stop criteria [137]. In this way, the GA algorithm can solve optimization problems with nonlinear equality and inequality constraints [137].

### C. OTHER OPTIMIZATION TECHNIQUES USED IN THE DESIGN OF SRMs

This subsection reviews the optimization techniques that are not categorized as stochastic or deterministic techniques and used for SRMs design. This includes the design of experiments, response surface method, and Taguchi's method. This part also discusses the concept of multi-objective optimization.

#### 1) DESIGN OF EXPERIMENTS METHOD

One of the time-efficient multi-objective optimization methods used for electrical machine design is the design of experiments method (DoE). DoE is a statistical optimization tool that effectively quantifies the effects of changing the geometrical design variables on the SRMs responses [112]. For a small number of design variables, the one factor at a time (OFAT) method is used. However, this method becomes impractical after a certain number of design variables as the number of FE evaluations increases exponentially with the number of design variables. As shown in Fig. 25, with only three variables and two levels for each design variable, eight FE evaluations are required with the OFAT method. In general, the number of process evaluations for this method is $L^n$, where L is the number of levels and $n$ is the number of the design parameters.

The central composite design (CCD) and the Latin hypercube design (LHD) methods are used to overcome the OFAT limitation on the number of parameters. In the CCD, the sample points are distributed at the center and the corners of the design space [138]. However, with a wide design space range, it is difficult for the CCD to gather the global response information of the electric machine [112]. The LHD covers the design space by random samples with the advantage of flexibility and better space-filling [139].

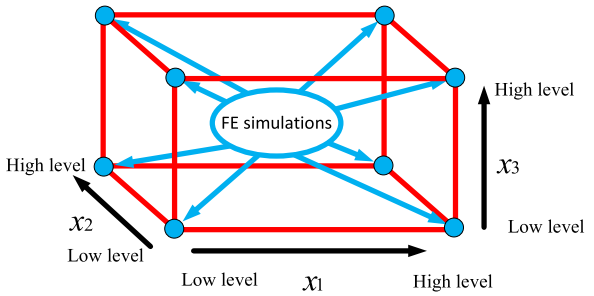


**FIGURE 25. An example of the number of FE simulations DoE required when using the OFAT method for three variables with two levels.**

#### 2) RESPONSE SURFACE METHOD

Another method used for multi-objective optimization is the response surface (RS) method. In the response surface method, the responses of the different objectives are evaluated at different points in space, then the response at any other point in the design space is evaluated by interpolation. The RS becomes the surrogate model of the SRM for multi-objective optimization using multi-objective optimization methods, such as PSO or GA [140].

#### 3) TAGUCHI'S METHOD

According to this method, the optimization process consists of four steps: planning, conducting, analyzing, and validating [141]. The method starts with the planning phase, where the design parameters are selected and the required simulations are determined. The method is based on an idea called orthogonal array to determine the number of simulations required for the optimization. Table 1 presents a typical orthogonal array used in an optimization process consisting of four parameters and three levels for each parameter. This array is called $L_9(3^4)$, which means that nine simulations need to be conducted to optimize four parameters with three levels.

The second phase of Taguchi's method is to conduct all the simulations planned in phase 1. The results are then analyzed to know the effect of each parameter on the objective function through a statistical study, and the best performance is selected [142]. Taguchi's method was utilized in the design of SRMs, and more details can be found in [142]–[144].

#### 4) MULTI-OBJECTIVE OPTIMIZATION DESIGN OF SRMs

As discussed in section III, different performance indices can be used as objective functions when optimizing SRMs. In multi-objective optimization, more than one performance index of SRMs are considered, and solution candidates are processed differently, as discussed in this section.

Most of the research efforts to improve the SRMs performance utilized only one objective function. However, improving only one performance metric at a time may have

**TABLE 1.** $L_9(3^4)$ Taguchi's method orthogonal array for four design variables: with three design levels for each variable.

| Simulation number | Design variables | | | |
|---|---|---|---|---|
| | A | B | C | D |
| *I* | *1* | *1* | *1* | *1* |
| *II* | *2* | *2* | *2* | *1* |
| *III* | *3* | *3* | *3* | *1* |
| *IV* | *3* | *2* | *1* | *2* |
| *V* | *1* | *3* | *2* | *2* |
| *VI* | *2* | *1* | *3* | *2* |
| *VII* | *2* | *3* | *1* | *3* |
| *VIII* | *3* | *1* | *2* | *3* |
| *IX* | *1* | *2* | *3* | *3* |

adverse effects on the other indices. On the other hand, multi-objective optimization provides a set of optimal solutions, which considers the behaviour of more than one performance index [145]. Therefore, multi-objective optimization can provide better SRM designs from different perspectives compared to the single-objective optimization to fit the needs of the different applications [112], [146].

The multi-objective optimization problems of SRMs can be described as follows:

$$\text{minimize: } \boldsymbol{f}(\boldsymbol{x}) \tag{35}$$

$$\text{Subject to: } g_k(\boldsymbol{x}) \leq 0, \quad k = 1, 2, \ldots m. \tag{36}$$

$$\text{Subject to: } h_j(\boldsymbol{x}) = 0, \quad j = 1, 2, \ldots l. \tag{37}$$

$$\boldsymbol{x}_{low} \leq \boldsymbol{x} \leq \boldsymbol{x}_{up} \tag{38}$$

where $\boldsymbol{f}(\boldsymbol{x}) = [f_1, f_2, \ldots\ldots\ldots f_h] : \boldsymbol{x} \rightarrow \mathbb{R}^h$ is the objective functions vector, $h$ is the number of objective functions, $\boldsymbol{x}$ is the design variable vector defined in the design space $\mathbb{R}^n$, $n$ is the number of the design parameters, whereas $\boldsymbol{x}_{up}, \boldsymbol{x}_{low}$ are the upper and lower boundary vectors of the design variables, respectively. The design space is subject to $m$ inequality constraints and $l$ equality constraints, as shown in (36) and (37), respectively.

In multi-objective optimization, the notation of "optimum" is called a "Pareto optimal solution". A multi-objective optimization solution is called a Pareto optimal solution or non-dominant solution if there is no way to improve one objective without adversely affecting one or more of the other objectives. The group of Pareto optimal solutions of the optimization problem is called the Pareto front set of solutions. A graphical representation of a multi-objective optimization solution of a two-objective function problem is shown in Fig. 26. The solutions A and B are non-dominant, whereas solution C is dominant. C is not an element of the set of the optimal solutions as other solutions can improve both objective functions simultaneously compared to the objective functions' values of solution C.

After defining the set of Pareto front solutions, a decision-making method should be used to select one of the Pareto front set elements as an optimal solution based on the design requirements. The decision-making process is based on the tradeoff between the different objectives to satisfy the design requirements [147].

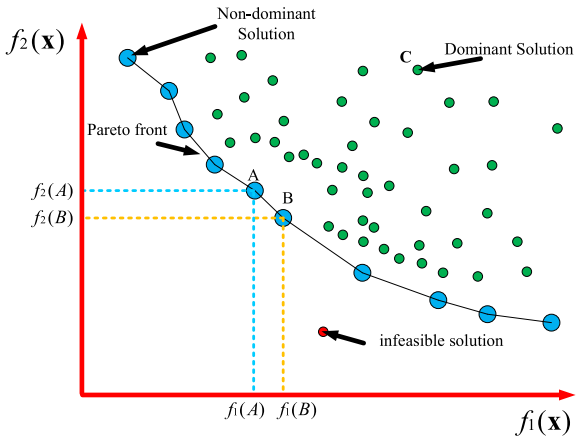


**FIGURE 26.** A graphical representation of the solutions of a two-objective optimization problem and the Pareto front set of solutions.

Stochastic optimization techniques such GA [115], [136], [148]–[150], PSO [151], [152], and SA [64], [115], were used for multi-objective optimization of SRMs in the literature. A more detailed literature review of the single-objective and the multi-objective optimization of SRMs is discussed in sections V and VI.

## V. GEOMETRY OPTIMIZATION OF SRMs

After reviewing the different deterministic and stochastic optimization methods used in literature for electric machines design, this section illustrates how these techniques were applied to enhance the performance of SRMs.

The geometry of electric machines is usually optimized to enhance performance. Fig. 27 shows the geometrical optimizable design parameters of SRMs. The parameters $h_s$ and $h_r$ are the length of the stator and rotor teeth, respectively. The parameter $y_s$ is the stator yoke thickness, whereas $y_r$ is the rotor yoke thickness. The parameters $\beta_s$ and $\beta_r$ are the arc angles of the stator and rotor teeth, respectively. The parameter $\theta_s$ represents the taper angle of stator teeth, whereas $\theta_r$ is the rotor teeth taper angle. The parameter $g$ is the airgap length and $R_{sh}$ is the shaft radius. The stator outer diameter and stack length are not commonly optimized since they are constrained by the application [153].

In [115], GA and SA were used to optimize the stator and rotor teeth arc angles, rotor diameter, and stack length of a 1 kW four-phase 8/6 radial-flux SRM to maximize the motor power density. The SA algorithm was able to achieve more than twice the power density increase achieved by GA [115]. However, SA required ten times longer time compared to GA.

The same geometric parameters were optimized in [64] to improve the power density of a two-phase 4/2 unidirectional radial-flux SRM by GA and SA. The SA algorithm was found to be more effective as it increased the machine power density by ∼27 % as compared to an 11.7 % increase using GA. The results show the fast convergence of the SA algorithm as compared to GA. Despite its superior performance, there

is no much-reported research on using SA in the geometry optimization of SRMs.

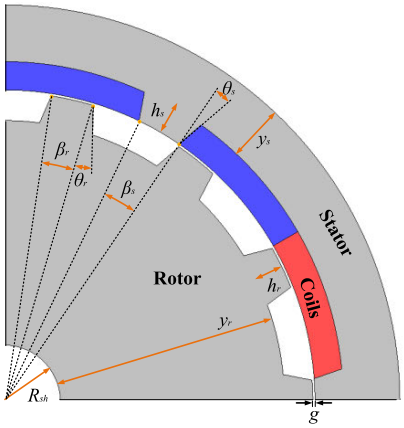


**FIGURE 27.** Main optimizable design parameters of SRMs.

In [154], a classic multi-objective PSO algorithm was applied to minimize the torque ripple and maximize the average torque of a four-phase 8/6 1.1-kW radial-flux SRM by optimizing the machine geometry. The considered geometric parameters are stator outer diameter, outer rotor diameter, stack length, air gap length, and stator and rotor teeth arc angles. The achieved results were compared to those of GA. The PSO increased the average torque by 5 % and reduced the torque ripple by 7 % as compared to the average torque and the torque ripple achieved by using GA.

A hybrid PSO-GA algorithm was applied to maximize the average torque and minimize the magnetic loss of a four-phase 8/6 radial-flux SRM [148]. The arc angles of the stator and rotor teeth and the thickness of the stator and rotor yokes were used in the optimization process. It was found that a proper selection of the weighting factors (C1 and C2 in equation (26)) and the acceleration factor $w$, increases the convergence rate of the PSO algorithm [148].

To decrease the computation time of FEA-based SRM optimization, the authors in [155] used an artificial neural network ANN-based model to predict and optimize the performance of a four-phase 8/6 3.7-kW radial-flux SRM. The rotor and stator teeth arc angles were optimized to increase the average torque and reduce the torque dip. The PSO and GA algorithms were used for the optimization problem. The GA algorithm increased the average torque by 27.9 % and reduced the torque dip by 34.4% as compared to the initial design. On the other hand, the proposed PSO algorithm increased the average torque by 29.1 % and reduced the torque dip by 34.7 % as compared to the initial design. The PSO algorithm also showed a faster convergence than the GA algorithm in this study.

In [156], the objective was to maximize both the average torque and the inductance ratio (to minimize the torque ripple) of a four-phase 8/6 3.7-kW SRM using PSO and GA. The inductance ratio is the ratio between the unaligned and aligned inductances. The PSO and GA increased the inductance ratio by 88.9 % and 85.9 % and the average torque by 29.1 % and 27.9 % as compared to the initial design, respectively. The PSO outperformed the GA in terms of design space exploration, speed of convergence, and robustness.

In [153], a multi-objective PSO (MOPSO) algorithm was used to simultaneously maximize the average torque, torque to copper loss ratio, and torque to motor active volume ratio (torque density). The considered optimization parameters are the stator and rotor pole arc angles. Weighting factors were used to provide a single objective out of the required three objectives. A prototype of the optimized motor was implemented, and a good match was found between the experimental and simulation results.

A novel multi-objective genetic particle swarm optimization algorithm (MOGPSO) was proposed in [151] to increase the torque density and efficiency of a three-phase 12/8 1.5-kW bearingless SRM (BSRM). The rotor yoke thickness, rotor pole height, and stator pole height and width were considered for the optimization process. The torque density increased by 287.6%, and the efficiency of the machine increased by 1.54% compared to the initial design. The process was based on an analytical model of the BSRM. The results were validated by FEA, where the analytical model showed a maximum error of 12.12 % as compared to the FEA model. The results showed that the proposed MOGPSO could search for more accurate non-dominated solutions in the Pareto front than the MOPSO [151].

The ant colony, artificial bee colony, and firefly algorithms are not commonly utilized to optimize the geometries of SRMs. Instead, they are used to optimize the control parameters of the machine drive circuit to increase the average torque and reduce the torque ripple [157]–[161]. A metaheuristic ant colony algorithm was used in [162] to maximize the average torque and efficiency of a three-phase 18/12 outrunner radial-flux SRM based on the motor analytical model. The optimization process considered five geometric parameters: the arc angles of stator and rotor teeth, the thickness of stator and rotor yokes, and rotor bore diameter. The average torque increased to 426.4 Nm, and the motor efficiency increased to 95.66% at the operating speed. A maximum error of 6.5 % was found between the analytical and FEA model results.

GA is prevalent in the geometry optimization of SRMs. It is very suitable for such an application due to the existence of many local minima that arise from the machine's nonlinearity [163], [164]. GA was used in [165] to maximize the torque of a three-phase 6/4 radial-flux SRM. The considered geometric parameters were the thickness of the stator and rotor yokes, shaft radius, height and arc angles of the stator and rotor teeth, air gap length, and stack length. The GA algorithm increased the average torque by 3.75 % higher than the heuristically optimized machine. In [164], GA was utilized to maximize the torque density of a 10-kW 48/50 low-speed slotted SRM (SSRM) for direct-drive wind energy generation. The optimization process was based on a 2D-FEA motor model to increase the accuracy at the expense of a longer optimization time. The thickness of the stator

and rotor yokes, in addition to the stator and rotor teeth parameters, were optimized.

The GA algorithm and the SQP algorithm were used to optimize three-phase 6/4 60 kW SRM to maximize the torque per ampere ratio of the machine in [181]. The GA optimization results showed that it is independent of the initial design. However, the SQP final design was changed by changing the initial design.

In [166], the Augmented Lagrangian Genetic Algorithm (ALGA) was compared to the parametric solution selection (PSS) method in optimizing a four-phase 8/14 radial-flux SRM based on a 2D FEM model of the machine. The objective is to maximize the average torque, torque factor (product of peak and average static torques of half electric cycle), loss factor (ratio of average torque to motor copper losses), torque density, and torque quality factor (ratio of average to peak static torques) and to minimize the torque ripple. The objective function was formed by the weighted sum of the different mentioned objectives. In the ALGA optimization, the considered parameters are the arc angles and taper angles of stator and rotor teeth, the thickness of stator and rotor yokes, and stator pole teeth height. Only stator and rotor teeth arc angles were considered in the case of the PSS optimization. The peak steady-state torque increased by 4.65 %, the average steady-state torque increased by 4.8 %, the torque factor increased by 7.02 %, the torque quality factor increased by 2.73 %, the torque density increased by 1 %, the loss factor increased by 38.59 %, and the torque ripple decreased by 2.34 % in the case of using ALGA compared to PSS. However, the comparison does not seem reasonable as the considered parameters are different in both cases.

Multi-objective GA optimization was used in [149] to optimize the geometry of a four-phase 24/18 18.6-kW SRM for an aerospace application. The stator and rotor teeth arc angles, outer rotor diameter, and stack length were optimized to increase the flux linkage to maximize the torque and the power per unit volume. The GA optimization results were compared to those resulting from a heuristic approach. The power density and maximum torque of the GA-optimized design are 13.97 % and 12.1 % higher than the heuristically optimized one.

The authors in [136] used the genetic fuzzy algorithm optimization method to maximize the efficiency and minimize the torque ripple of a four-phase 8/6 4-kW radial-flux SRM. As previously explained, the conventional GA algorithm selects the parents based on a probability function that gives the fittest individuals more chance to produce offspring from their chromosomes. The objective functions are combined with fuzzy weights in [136] to ensure that the fittest individuals for all objective functions have the highest probability of being selected. Nine different geometric parameters and the number of turns per phase were considered in the optimization process. The method improved motor performance as the efficiency increased by 4 %, and the torque ripple decreased by 18 % compared to the initial design.

In [167], a kriging-method-based surrogate model of a two-phase unidirectional 4/2 SRM was used to reduce the optimization time of the Pareto archived evolution strategy algorithm by reducing the number of the FEA simulations. The objective was to minimize the torque ripple and maximize the starting torque per phase. Each rotor tooth was divided into two parts of different heights in this design, as shown in Fig. 28. The considered optimization parameters are $\beta_0, I_{g1}$ and $I_{g2}$. This procedure increased the starting torque by 25% and reduced the torque ripple by 57.6 % compared to the initial design.

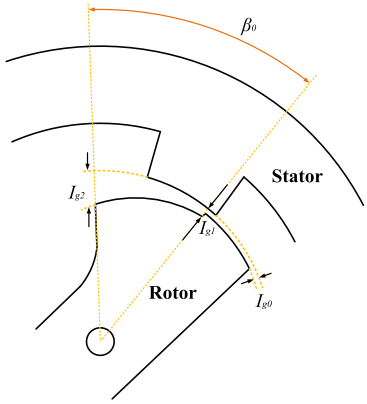


**FIGURE 28.** The optimizable geometric parameters in [167].

The complexity of multi-variable geometry optimization of a 12/8 low-speed SRM, used in micro electric vehicles, was minimized in [168] using a subset quasi-orthogonal algorithm. The algorithm optimizes the outer rotor diameter, arc angles of stator and rotor teeth, and stator and rotor yoke thicknesses to minimize the torque ripple and maximize the average torque. The proposed optimization technique comprises four steps. The constraints were first determined. Then, the sensitivities of the torque and torque ripple to the considered parameters were obtained. Thirdly, the multi-variable optimization problem was divided into three subsystems according to the sensitivity with respect to the parameters. Finally, subsystem optimization was sequentially performed. A significant drawback of this procedure is that the sensitivities were calculated once based on the initial design. The change in the sensitivities, as the design changes, was not considered. The torque ripple decreased by more than 40 %, and the average torque increased by more than 8 % compared to the initial design.

The concept of reducing the number of design variables based on their sensitivities was also presented in [112]. Based on the sensitivity analysis of the torque density, efficiency, and torque ripples to the different design parameters, the number of design parameters decreased from 13 to 6. The 6 design parameters are selected based on their objective function sensitivity.

The authors of [169] utilized a Pareto-based multi-objective differential evaluation method to maximize the static torque, efficiency, and torque per volume of a

**TABLE 2. Summary of the reviewed studies and some other studies about geometry optimization of SRMs.**

| Reference | Machine Configuration | Optimization | | Objective Function | | | | | Experimental Validation of the Design |
|---|---|---|---|---|---|---|---|---|---|
| | | Optimization Type | Optimization Method | Average Torque | Torque Ripple | Torque Density | Radial Force | Efficiency | |
| [115] | 4-phase 8/6 | Geometry | SA/GA | - | * | * | - | - | No |
| [153] | 4-phase 8/6 | Geometry | DoE | * | - | * | - | * | Yes |
| [173] | 3-phase 6/4 | Geometry | N/M | * | - | - | - | * | No |
| [136] | 4-phase 8/6 | Geometry | GA | - | * | - | - | * | No |
| [174] | N/M | Geometry | Response surface | - | - | - | - | * | No |
| [63] | 3-phase 6/14 | Geometry/ topology | Interior point method& On/off topology optimization | * | * | - | - | - | No |
| [150] | 3-phase 12/8 | Geometry | GA | * | * | - | * | - | No |
| [156],[154], [148],[155] | 4-phase 8/6 | Geometry | PSO&GA | * | * | - | - | Only in [150] | No |
| [78] | 4-phase 8/6 | Geometry | Trial and error using FEA software | - | - | - | * | - | Yes |
| [151] | 3-phase 12/8 | Geometry | Genetic PSO | - | - | * | - | * | No |
| [162] | 3-phase 18/12 | Geometry | Ant Colony | * | - | - | - | * | No |
| [164] | 3-phase 12/64 | Geometry | GA | - | - | * | - | - | No |
| [165] | 3-phase 6/4 | Geometry | GA | * | - | - | - | - | No |
| [166] | 4-phase 8/14 | Geometry | ALGA | * | * | * | - | * | No |
| [149] | 4-phase 24/18 | Geometry | GA | * | - | * | - | - | No |
| [136] | 4-phase 8/6 | Geometry | GFA | - | * | - | - | * | No |
| [167] | 2-phase 4/2 | Geometry | N/M | * | * | - | - | - | No |
| [152] | 4-phase 8/6 | Geometry | PSO | * | * | - | - | - | No |
| [175] | 3-phase 12/8 AFSRM | Geometry | Trial and error using FEA software | * | - | - | - | - | Yes |
| [176] | LSRM | Geometry | EA | * Force | * Force ripple | * Force density | - | - | Yes |
| [177] | LSRM | Geometry | Proposed technique | * Force | * Force dip | - | - | - | Yes |
| [178] | 4-phase 8/6 | Geometry | Penalty/Lagrangian methods | - | * | - | - | - | No |
| [179] | 3-phase 12/8 | Geometry | Trial and error using FEA software | * | * | | | * | Yes |
| [180] | LSRM | Geometry | N/M | * Force | Force dip | * Force density | - | - | No |
| [181], [182] | 3-Phase 6/4 | Geometry | SQP/GA methods | * | - | * | - | - | No |
| [140] | 4-phase 8/6 | Geometry + control | CCD+RS+GA | - | * | - | - | * | No |
| [112] | 3-phase 6/10 | Geometry | PSO & DoE | * | * | - | - | * | No |
| [143] | 4-phase 16/14 | Geometry | Taguchi method | * | * | - | - | * | Yes |
| [183] | LSRM | Geometry | N/M | * Force to copper mass | - | * Force density | - | - | Yes |

* Considred as an objective function.
- Not considred as an objective function.
N/M Not mentioned in the article.
R Radial-flux SRM.

three-phase 18/12 outer-rotor radial-flux SRM for in-wheel EV application. The considered parameters are stator outer diameter, stator and rotor teeth arc angles, and stator and rotor yokes' thicknesses. In the Pareto-based optimization, the algorithm provides a set of nondominant solutions and level the selection process to the decision-maker [169]. An analytical model of the SRM was used in the optimization process to reduce the computational time. The optimized design was validated numerically, using 3D FEA simulations, and experimentally.

The average torque and the inductance ratio coefficient of an 8/6 SRM were maximized in [152] using a PSO method with an adaptive accelerating factor. The stator and rotor outer diameters, stack length, airgap thickness, and the arc angles of stator and rotor teeth were considered. The PSO optimization method was able to increase the average torque by 32.5 % and decrease the torque ripple by 34.97 % compared to the initial design.

The GA algorithm was used to maximize efficiency and minimize the torque ripple of a four-phase 8/6 4-kW SRM [136]. The stator and rotor outer diameters, number of phase turns, air gap length, the thickness of stator and rotor yokes, and the height and arc angles of the stator and rotor teeth were considered in the optimization process. A magnetic equivalent circuit model of the machine was used to reduce the optimization time. The objective functions

were joint with fuzzy membership functions such that the fittest chromosomes for all objective functions have a higher probability of continuing to the next generation [136]. However, the other chromosomes could be considered in the next generation according to their fuzzy weights [136]. The fuzzy expert performance predictor is designed based on a sensitivity analysis of the motor parameters [136].

In [170], an interior-point optimization algorithm used the adjoint-based sensitivities to optimize the geometry of a 6/14 radial-flux SRM to maximize the machine static torque characteristics. The considered parameters were rotor teeth height, stator yoke thickness, rotor yoke thickness, stator pole arc angle, rotor pole arc angle, stator teeth taper angle, and rotor teeth taper angle. The average value of the static torque half-cycle increased by 33.52% compared to the initial design.

The average torque and torque per inertia of a four-phase 8/6 SRM for high-acceleration applications were maximized in [171] using one factor at a time (OFAT) design of experiments optimization. OFAT is a method of designing experiments that simulates one parameter change at each step instead of multiple factors. It does not require previous knowledge about the optimization problem. However, the number of simulations needed increases exponentially with the number of design parameters [113].

In [172], Taguchi method was used to decrease the required number of simulations and the simulation time. Eight geometric parameters were considered in the optimization process [171]. After 2189 simulations, the peak static torque increased by 5 %, and the average static torque increased by $\sim 2$ % compared to the initial design.

The influence of different stator and translator geometric parameters of planar and tuber LSRMs on the electromagnetic force and electromagnetic force ripples were studied in [183] and [184]. In [183], the number of phases, pole stroke (distance covered by the translator's teeth from two consecutive aligned positions when two successive phases are excited), and the current density were optimized to maximize the force per copper mass and the force density of a longitudinal flux double-sided LSRM. The force density increased by 132%, and the force per copper mass increased by 78% compared to the initial design.

The study in [184] shows that increasing the translator pole width of single-sided LSRM, Fig. 10, increases the trust force but decreases the specific force of the machine at the same time. The study also shows that increasing the translator pole pitch increasing the trust force but increases the cogging force at the same time. The stator pole width has to be carefully selected to maximize the average trust force and minimize the force ripples of that machine [184]. The effect of the stator pole shoe shape of the single-sided LSRM is also discussed in [184]. One way to maximize the thrust force and minimize the force ripple is to optimize the skew and taper angles of stator poles [184]. One of the critical parameters of the LSRM is the airgap length, the length of the gap between the translator and the stator. The length reduction increases the trust force but increases the force ripple at the same time, so this parameter should be carefully optimized based on the application needs [184].

In [176], an EA-based optimization algorithm was used to optimize the stator and translator pole width and height and stator yoke thickness of a double-sided longitudinal-flux LSRM. The optimization objective was to achieve a low mass to force ratio and improve the force quality for vertical-motion applications. The mass-to-force ratio was decreased by 8.15 %, and the force ripple decreased by 76.5 % compared to the initial design.

The authors of [177] used the different geometrical parameters sensitivities to minimize the force dip ratio and to maximize the active payload ratio of a segmented-stator single-sided planar LSRM. A high payload ratio means a high on-load capacity, which indicates a high conveyance efficiency. The distance between two stator segments, translator pole width, translator pole tip width and height, and the stator segment slop angle are the parameters used for optimization. The payload ratio increased by 43.8 %, and the force dip ratio decreased by 21.3 % compared to the machine's initial design.

In [153], the one factor at a time DoE was used to optimize the stator and the rotor pole arc angles of an inner-stator outer-rotor 8/6 SRM with four-level for each variable to maximize the mean torque, mean torque per copper loss ratio, and torque density. The weighted average method was used to select the solution that satisfies the design requirements.

In [140], the central composite design (CCD) method was used to build the response surface models of the torque ripple and efficiency of a four-phase 8/6 inner-rotor SRM. The design variables were stator and rotor pole arc angles and phase turn-off angles. A multi-objective GA method was used to minimize the torque ripple and maximize the motor efficiency. Finally, the Pareto front was drawn to select the optimal solution. The torque ripple decreased by 33.25%, and the motor efficiency increased by 3.43 % compared to the initial design.

Geometry optimization was used in the literature for SRMs core losses reduction. In [173], the tooth width to pole arc angle ratio, the rotor diameter to the machine outer diameter ratio, and the pole arc angle to the airgap length ratio were used to minimize the torque per ohmic loss and maximize the efficiency of a three-phase 6/4 SRM. The stack length, the airgap thickness, and the number of turns were optimized in [174] to maximize the machine efficiency of an SRM. The efficiency of the considered machine increased to 86%.

These studies and more are summarized in Table 2 to give the reader an overview of the methods and the objective functions that were used in the literature for SRMs geometry optimization.

## VI. TOPOLOGY OPTIMIZATION OF SRMs

In geometry optimization, geometric parameters, such as those shown in Fig. 27, are optimized to enhance the machine performance. The number of design parameters is fixed in

geometry optimization, and the geometry follows a predetermined template. Another type of optimization, topology optimization (TO), allows the topology of the structure to evolve to a new topology in an iterative way. For example, flux barriers inside the rotor or the stator design spaces could be added and optimized for performance improvement [185], [186], [187]. These barriers increase the number of optimizable parameters if geometry optimization is used, which increases computation time and complexity [188]. Also, geometric parameterization and optimization of flux barriers are not flexible to reach the best shape [188]. Topology optimization provides more smooth barrier designs as it allows a flexible material distribution in the considered domain to achieve the objective functions [189]. An example of the flux barrier design in SRM is shown in Fig. 29.

Several published articles use topology optimization to improve SRMs performance. Topology optimization was first applied to SRMs in [190] to maximize the machine magnetic energy profile. It was then used in [191] to reduce the vibration caused by the magnetic forces. In [192], it was applied to the rotor and stator poles of a 6/4 SRM to reduce the torque ripples.

This optimization type could lead to novel SRM geometries [192], [193]. Manufacturability constraints could be added to the optimization problem to ensure the feasibility of the design. Additive manufacturing (AM) could also help to manufacture resulting complex shapes [194].

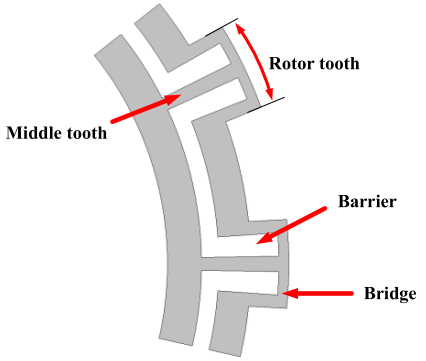


**FIGURE 29.** A rotor flux barrier design for 6/14 radial flux SRM.

Fig. 30 shows various topology optimization methods were used for the performance improvement of electric machines in the literature. TO methods are classified into two main categories: gradient-based and non-gradient-based methods.

The level set method is a gradient-based TO method. It gives a more feasible solution but with a slower convergence as compared to the material-density-based method [195]. The design space and boundaries are represented with a level set continuous function [196]. For a given design space S with a boundary B, as shown in Fig. 31, the level set function is given as follows:

$$\begin{cases} \varphi(x,y) > 0, & \text{Magnetic material} \\ \varphi(x,y) = 0, & \text{Boundary edge} \\ \varphi(x,y) < 0, & \text{Air.} \end{cases} \tag{39}$$

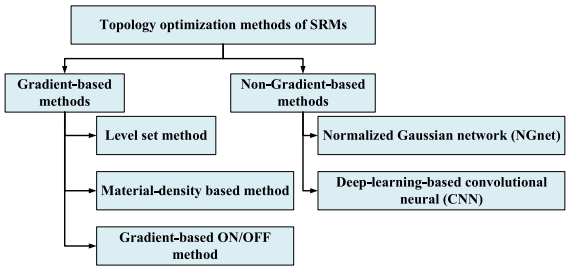


**FIGURE 30.** Main topology optimization methods of SRMs.

The objective of the level set topology optimization is to find the value of $\varphi(x, y)$ at each location $(x, y)$ and to effectively distribute the material on the design space to satisfy the design objectives. The method usually falls into local optima as it relies on the sensitivity of the different design space elements [197].

The level set method was used in [195] to increase the torque to mass ratio of an 8/6 SRM. The TO applied to the rotor region in this study was able to increase the torque density of the motor by 7.75 %. This was, however, coupled with a reduction of the mean torque by 1.2% as compared to the reference design.

Another topology optimization technique called Material-density-based methods or method of moving asymptotes was used for SRMs design [198]. Material-density-based methods have faster convergence than the level set method [195], [199]. The objective function is minimized by defining the material type (air or ferromagnetic material) based on the value of the density function $\rho_i$ of the $i^{th}$ element as follows:

$$\rho_i \begin{cases} 1, & i \in \Omega_m \\ 0, & i \in \Omega_a \end{cases} \tag{40}$$

where $\Omega_m$ and $\Omega_a$ are the ferromagnetic and air regions, respectively. Although the material status should be either 0 or 1, the method allows the density function to be continuous between 0 and 1 by replacing the density function in (40) with a smooth Heaviside function $\rho(\psi)$, defined by an auxiliary optimization variable, $\psi$ [199]. This procedure helps to make the density function continuous and prevent discontinuity [194]. However, as shown in Fig. 32, it leads to gray elements whose material does not exist in reality. In the auxiliary optimization variable method [199], the density is described by a smoothed Heaviside function with a switch level:

$$\rho(\psi) = \frac{3}{16}\left(\frac{\psi}{h}\right)^5 - \frac{5}{8}\left(\frac{\psi}{h}\right)^3 + \frac{15}{16}\left(\frac{\psi}{h}\right) + \frac{1}{2}, \quad (-h \le \psi \le h), \tag{41}$$

where $h$ is the half of the switch width between $\rho(h) = 1$ and $\rho(-h) = 0$.

The magnetic reluctivity of the $i^{th}$ element is then defined as follows [195], [200]:

$$\upsilon_i(\psi_i, |B^2|) = (1 - \rho(\psi_i))^p * \upsilon_{air} + (\rho(\psi_i))^p * \upsilon_F(|B^2|), \tag{42}$$

where $\upsilon_i$, $\upsilon_{air}$, and $\upsilon_F$ are the reluctivity of the $i^{th}$ element, the reluctivity of air, and the reluctivity of ferromagnetic material, respectively. $\upsilon_F$ is a function of the square of the flux density $B$ at that element. The variable $p$ is the penalization coefficient. The proper selection of $p$ prevents the presence of gray elements with $0 < \rho_i < 1$. $p$ was suggested to be equal to 3 in [200] to ensure good convergence to the white and black elements with a small number of gray elements.

In [195], material-density-based TO resulted in thin parts that need to be structurally evaluated. A material-density-based TO exploiting sequential linear programming was used in [192] to minimize the torque ripple of a three-phase 6/4 radial-flux SRM. The considered design space included the rotor and part of the stator teeth. The torque ripple decreased to 27% compared to a torque ripple of 245% for the initial design.

The authors of [194] used the method of moving asymptotes to optimize the rotor teeth topology of a four-phase 8/6 radial-flux SRM to maximize the average torque and reach the target torque for two different applications. After optimizing the two motors, the torque of the final designs reached target torque of 0.12 and 0.16 N.m.

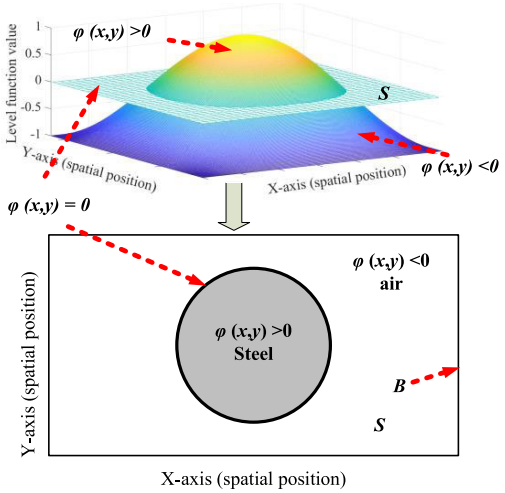


**FIGURE 31.** A level set function and the corresponding material distribution in the design space.

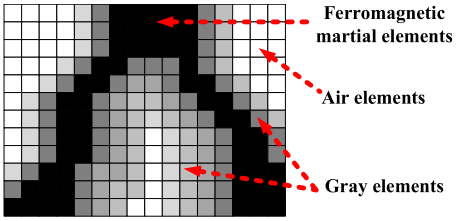


**FIGURE 32.** The design space after material-density-based TO optimization.

The authors of [201] used a gradient-based ON/OFF TO method in designing electromagnetic devices for the first time. The method is based on the objective function sensitivity with respect to the reluctivity of each element in the design space [201], [202].

Fig. 33 shows a flowchart of the method. The algorithm starts by evaluating the objective function value of the initial SRM topology. Then, the objective function sensitivities are computed with respect to the reluctivity of the elements of the design space [63]. Ferromagnetic material and air are assigned to elements with positive and negative sensitivities, respectively. This applies to the highest-sensitivity elements until the allowable number of designable elements $N$ is attained. Designable elements are those elements inside the design space allowed to change their material. If the objective function value decreases, the topology changes and the new topology sensitivities are calculated. However, if the objective function value increases, $N$ decreases in the annealing process. The overall process continues until $N$ reaches zero.

The gradient-based ON/OFF topology optimization deals with a large number of design variables and has faster convergence characteristics than the material-density-based method [201]. This topology optimization has less computational time than GA-based ON/OFF topology optimization, but it may terminate at a local optimum solution, unlike GA.

A gradient-based ON/OFF topology optimization was used to minimize the torque ripple of a 6/14 SRM for Heating, Ventilation, and Air Conditioning (HVAC) application in [63]. A part of the stator tooth was considered as the design space. The torque ripple gradients to all the design space elements were computed using the discrete adjoint variable method [202]. The motor torque ripple was reduced by ∼14%, but the average torque also slightly decreased since the introduced flux barriers reduced the machine flux linkage.

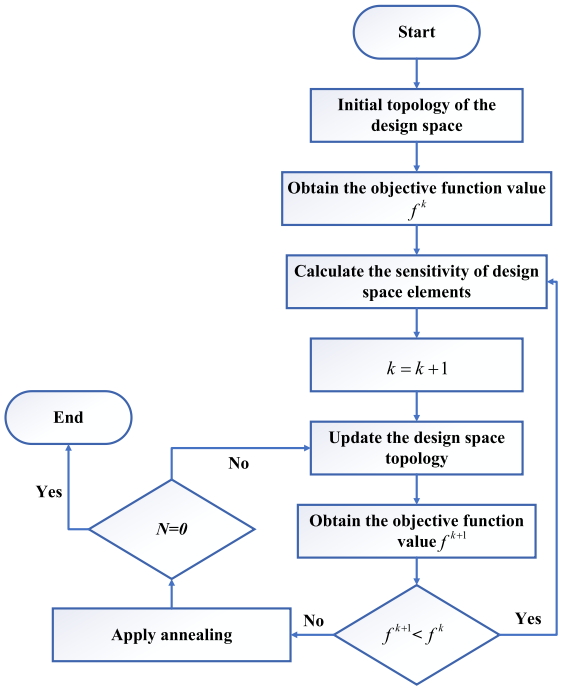


**FIGURE 33.** A flowchart of gradient-based ON/OFF TO optimization method.

The main disadvantage of gradient-based topology optimization is the difficulty of evaluating non-differentiable

objective functions such as iron losses [188]. A non-gradient-based ON/OFF topology optimization, also known as stochastic topology optimization, can be applied in this case [197], [203]. This approach does not require any gradient information [204], but it may result in unacceptable and complex shapes with isolated magnetic regions, as shown in Fig. 34 [205], [206]. In [157], the authors proposed the immune algorithm that overcame this issue and produced a TO-based manufacturable design. Fig. 35 shows a flowchart of the ON/OFF TO with the immune algorithm. The algorithm is based on the mammalian immune system [197]. It starts with evaluating an N number of initial solutions called antibodies. If any solution satisfies the termination condition, it will be selected as the final solution. If this is not the case, P % of the low-ranked antibodies will be eliminated. Several clones are created for each survived antibody based on its rank; more clones are developed as the rank increases. The affinity maturation process is then applied to the different clones. Different clones are modified by changing the material in the surrounding elements of some random nodes to air or steel, as shown in Fig. 36. *P* % of antibodies is randomly generated, and the process repeats. This algorithm was used to optimize the topology of the rotor of an SRM to maximize the average torque in [207].

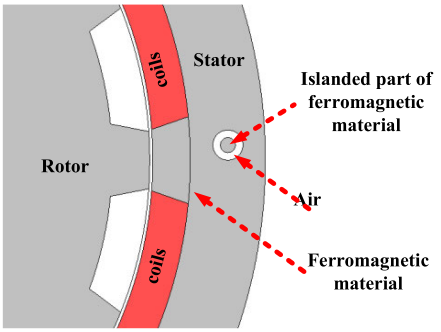


**FIGURE 34.** An example of an islanded region during topology optimization.

Another non-gradient-based TO method is the Normalized Gaussian Network (NGnet) [206]. This method avoids isolated elements and leads to smooth manufacturable structures [188]. The design space is divided into Ncells number of cells (elements). Each cell's state is defined by the NGENT function's output that is determined based on the weighted sum of the normalized Gaussian function. The output of the NGnet is obtained from:

$$y(\boldsymbol{x}) = \sum_{i=1}^{N} w_i b_i(\boldsymbol{x}), \tag{43}$$

$$b_i(\boldsymbol{x}) = \frac{G_i(\boldsymbol{x})}{\sum_{j=1}^{N} G_j(\boldsymbol{x})}, \tag{44}$$

where $G_i(\boldsymbol{x})$ is a Gaussian function at the location $\boldsymbol{x}$. The variables $i$ and $j$ represent cell indices, and $w_i$ is the weighting coefficient of the normalized function $b_i(\boldsymbol{x})$. The state $S_c$ of

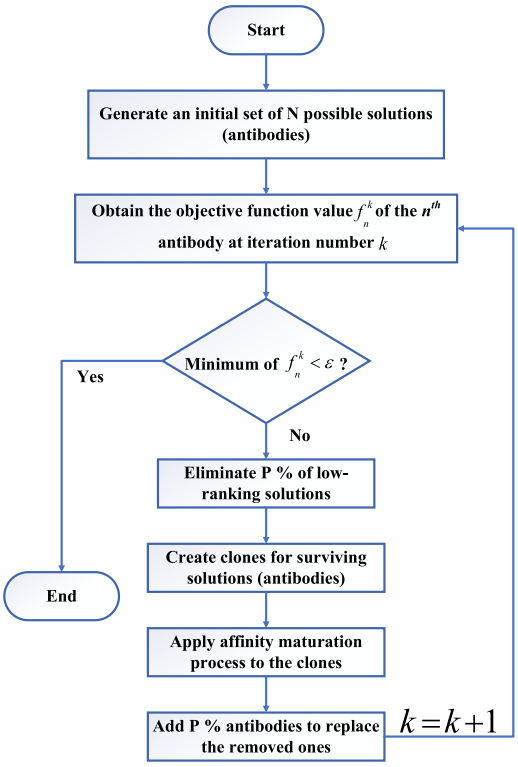


**FIGURE 35.** A flowchart of the ON/OFF TO method with the immune algorithm.

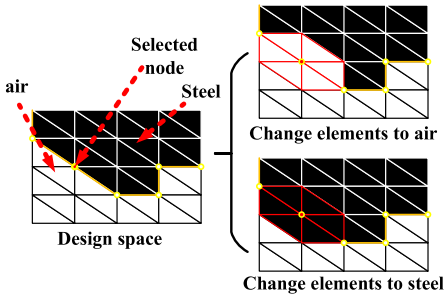


**FIGURE 36.** Changing the elements' states in the affinity maturation process.

cells is determined from:

$$S_c = \begin{cases} \text{on} & y(\boldsymbol{x}_c) \geq 0, \\ \text{off} & y(\boldsymbol{x}_c) < 0. \end{cases} \tag{45}$$

where $\boldsymbol{x}_c$ is the center of cell $c$. When the state of the cell is on, its material is set to iron, whereas the material is set to air when the state is off.

Fig. 37 shows the process of determining the state of each cell's based on the weighted sum of the associated normalized Gaussian function. The NGnet topology optimization requires substantial computational cost as FEA-based computation is needed at each generation [208].

To the authors' best knowledge NGnet was not used for SRM topology optimization. However, this method showed a significant performance improvement for other types of electrical machines such as Synchronous reluctance motor [188] and interior permanent magnet motor [208]. This

is considered a potential opportunity to enhance the performance of SRMs by using the NGnet topology optimization method in the future. The drawback of this method is the high computational cost, as indicated in [208].

Recently, topology optimization gained more attention thanks to the additive manufacturing technologies that allow manufacturing more complex shapes than traditional manufacturing [194], [195], [209]. Topology optimization results in a honeycomb structure of the rotor and stator. This structure is complicated to be realized by traditional manufacturing methods [194]. The complete process, including design optimization, 3D printing of the SMC parts, and assembly, was investigated in [194], [210]. In [211], additive manufacturing was used to manufacture a complex rib structure rotor for a three-phase 6/4 SRM with a novel rotor structure to minimize the torque ripple and the windage loss. The torque ripple of that motor decreased by 35.8 % compared to the original design without the complex structure rib. Besides, the windage loss decreased by introducing a thin rib on the outer part of the rotor.

On the other hand, the change in the material properties due to the additive manufacturing process should be considered. Additive manufacturing and 3D printing of the optimized parts change the material magnetic, electric, and mechanical characteristics [212]. Eddy-current loss in the 3D printed solid cores is higher than that of the laminated cores [194]. In [194], the author depends on selecting an SMC material that has the highest possible resistivity to limit the eddy current loss of the optimized part.

Topology optimization is sensitive to mesh density and material *B-H* characteristics [195]. Representing the material with a linear reluctivity model and decreasing the mesh density decreases the optimization time; however, the optimized machine performance accuracy decreases, and the optimized shape becomes coarse [195]. [213], it was concluded that different material reluctivity models, linear and nonlinear, lead to different results. This can be addressed by using a section of the machine with symmetrical boundaries.

A summary of the studies that used topology optimization for improving the performance of SRMs in the literature is organized in Table 3.

## VII. TOPOLOGY OPTIMIZATION BASED ON DEEP LEARNING

Machine learning is used for electrical machines optimization through automating surrogate model building within the optimization loop [214]. Using surrogate models reduces the ON\OFF or GA-based topology optimization time. Different surrogate models can be used based on different methods such as the response surface method [215], [216], kriging method [217], space mapping method [218], artificial neural network method [219], and convolutional neural network [208]. In that way, the optimization method time can be reduced significantly.

Many machine learning methods were used in literature for electric machine design. These methods include deep learning, random forest technique, extreme learning, support vector machines, and artificial neural network. The deep-learning-based convolutional neural network (CNN) was used in literature for the topology optimization of electric machines. However, to the authors' best knowledge, no machine learning method was used for SRM topology optimization. This section reviews the effectiveness of machine learning on optimizing other types of electric machines to show that it could be a potential opportunity for enhancing the topology optimization of SRMs.

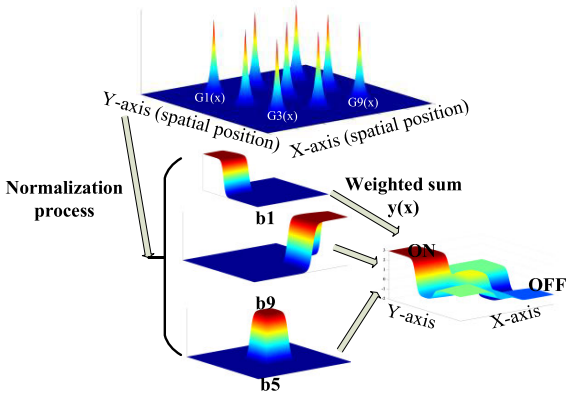


**FIGURE 37.** The output of the NGnet weighted sum function in the case of nine Gaussian functions for nine cells.

In [208], deep learning was used to reduce the NGnet topology optimization computational burden and time of interior permanent magnet motor (IPM motor) design optimization. The algorithm is divided into learning and optimization phases. In the learning phase, the training data was developed by performing a preliminary topology optimization using a small number of individuals (design elements). The motor 2D images were used to train a convolutional neural network (CNN).

In the optimization phase, the convolutional neural network was used to replace the FEA. The CNN was trained to classify different motor models based on the model performance index, such as motor efficiency, average torque and torque ripple. If the performance index is low, such as low average torque or high torque ripple, the CNN is used for motor performance evaluation; However, if the motor performance is predicted to be high, FEA of the motor topology is performed for motor performance evaluation. With this technique, the number of FEA execution for NGnet reduced by around 30% [208].

There are two feasible deep learning techniques for topology optimization computational acceleration: online and offline techniques [209], [213]. The former technique performs the training process during the optimization phase, whereas the latter performs the learning phase first. The method used in [208] is illustrated in Fig. 38. The red path in the figure represents the preliminary process for the initial CNN training. The green path represents the evaluation of the design performance within the optimization loop based on CNN. The yellow path represents categorizing the

**TABLE 3. Summary of the studies used topology optimization for improving the performance of SRMs in the literature.**

| Reference | Machine configuration | optimization | | Objective function | | | | | Exp. validation of design |
|---|---|---|---|---|---|---|---|---|---|
| | | Optimization method | Design space | Average torque | Torque ripple | Torque density | Radial force | other | |
| [63] | 3-phase 6/14 | Interior point method& On/off topology optimization | Stator poles | * | * | - | - | - | No |
| [191] | 3-phase 6/4 | level set method | The stator | - | - | - | * | Minimize frequency response of the stator structure | No |
| [192], [198], [220] | 3-phase 6/4 | material-density-based TO | Stator teeth and rotor | - | * | - | - | - | Yes in [220] |
| [207] | 3-phase 24 slot and new rotor topology | ON/OFF TO with immune algorithm | The rotor | * | * | - | - | - | No |
| [221] | 4-phase 8/6 | level set method | Rotor poles | * | * | - | - | - | No |
| [195] | 4-phase 8/6 | Material-density-based methods (GCMMA) | Rotor poles | * | - | - | - | Minimize mass | No |
| [64] | 3-phase 6/4 | ON/OFF TO based on GA and SA | -Rotor -Stator -Copper | * | - | - | - | - | No |
| [194] | 4-phase 8/6 | Material-density-based methods | Rotor poles | * | * | - | - | - | No |

* Considered as an objective function.
\- Not considered as an objective function.

performance evaluated by CNN to check the probability of FEA evaluation requirement. The blue path represents the FEA of the design and the possibility of using this evaluation on the online training of CNN.

The main problem of CNN is that it requires a large number of data points for the training process prior to the optimization process [223]. The authors in [223] proposed a method for CNN training based on transfer learning which required a small number of data for the training process. In this method, a single VGG-16 CNN, which is CNN trained with 1.2 million learning data and composed of 1000 different classes [224], was used as a surrogate model for two different IPM motors. The preliminary training data was obtained from a GA topology optimization with a small population size of two different IPM motors with variations in the rotor structure. The motor performance is shown to be correctly inferred by the transfer learning with small data used for learning. In the optimization stage, the CNN was used to evaluate all the individuals of the GA optimization except the Pareto front individuals evaluated by FEA. The method was used to optimize two different IPM motors with different rotor structures. The computational cost of the GA-based topology optimization was reduced to 15% using CNN with transfer learning concept compared to the conventional GA method where FEA is used for fitness evaluation for all individuals.

In [225], the number of the required finite element electromagnetic evaluations of the target machine was reduced by 50% compared to the number required by GA-based topology optimization. An initial topology was optimized first by GA with a small population size to train the CNN. The CNN is then used as a surrogate model in the main topology optimization with large population size. This technique reduced the number of finite element simulations by 50% compared to GA-based topology optimization.

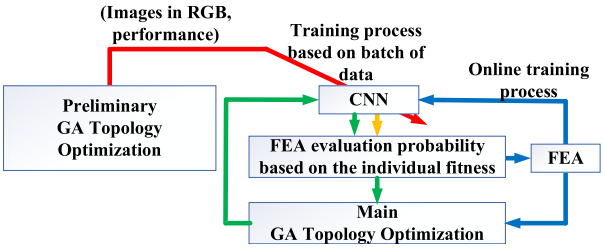


**FIGURE 38. A flowchart of topology optimization based on offline trained CNN for electric machine design.**

## VIII. TRENDS AND OPPORTUNITIES

There is currently increasing interest in the geometry and the topology optimization of SRMs to address the machine limitations such as high torque ripple, low average torque, and high acoustic noise. That will help widen the application areas of SRMs. Design optimization of SRMs configurations like the axial flux SRMs and LSRMs were not covered well in the literature, and the number of publications that covered this area is around 10% of the total publications of SRMs optimization (covered in this research). The authors expect an increase in these percentages in the future due to the advantages of these configurations.

In general, according to our research, the number of publications for topology optimization of SRMs is around 20% of the total publications of the SRMs design optimization. The authors of this review study believe that this percentage will increase in the future due to the effectiveness of the topology optimization and the significant advance in additive manufacturing.

On the other hand, CNN deep learning shows a significant reduction in the topology optimization time of electrical machines; however, it was not used for SRMs design yet. It is currently trending as a non-gradient-based topology optimization method and could be a research opportunity to use such a technique in SRM performance improvement.

There are abundant opportunities for topology optimization techniques like NGnet and non-gradient-based ON/OFF methods for SRMs topology optimization. These methods show a significant performance improvement for other types of electric machines, and according to our best knowledge, these methods have not been used yet for SRMs design optimization. These techniques are considered an excellent opportunity to improve the performance of the SRMs.

## IX. CONCLUSION

The paper provides a comprehensive review of different optimization techniques used to enhance SRMs performance metrics. The paper starts with a brief discussion about various configurations of SRMs. Radial and axial, rotating and linear, and other categories are reviewed.

Then, the paper investigates deterministic and stochastic optimization procedures. The main techniques under each category used for SRMs optimization are explained. Although deterministic optimization techniques are faster than stochastic techniques, the latter guarantee achieving a globally optimum solution. Unlike stochastic optimization, deterministic optimization requires the gradients of the objective functions with respect to the design parameters. Finite difference and adjoint variable methods could be used to calculate these gradients. Although the finite difference methods are accurate with acceptable error, they are computationally expensive compared to the less accurate adjoint variable methods.

After reviewing the performance metrics of SRMs that were used as objective functions in literature, the paper then reviews the geometry optimization of SRMs to improve these objective functions.

Finally, the topology optimization of SRMs is reviewed, and most of the topology optimization methods used for SRMs performance optimization are reported. Topology optimization could result in complex shapes. Different techniques that solve this issue were reported. Besides, additive manufacturing makes achieving TO-based intricate designs easier.

Topology optimization techniques are very time-consuming processes. There is abundant opportunity to decrease its time by using CNN deep learning, which is not covered in the literature. The CNN deep learning showed a significant reduction in the topology optimization of electrical machines such as PMSM, and it is recommended to investigate its performance with SRMs.

## ACKNOWLEDGMENT

The authors thankfully acknowledge Powersys Solutions for their support with JMAG software in this study.

## REFERENCES

[1] N. Zabihi and R. Gouws, "A review on switched reluctance machines for electric vehicles," in *Proc. IEEE 25th Int. Symp. Ind. Electron. (ISIE)*, Santa Clara, CA, USA, Jun. 2016, pp. 799–804.
[2] B. Bilgin, A. Emadi, and M. Krishnamurthy, "Comprehensive evaluation of the dynamic performance of a 6/10 SRM for traction application in PHEVs," *IEEE Trans. Ind. Electron.*, vol. 60, no. 7, pp. 2564–2575, Jul. 2013.
[3] H. Shin and K. Lee, "Optimal design of a 1 kW switched reluctance generator for wind power systems using a genetic algorithm," *IET Electr. Power Appl.*, vol. 10, no. 8, pp. 807–817, Sep. 2016, doi: 10.1049/iet-epa.2015.0582.
[4] C.-T. Liu, Y.-M. Chen, and D.-C. Pang, "Optimal design of a micro axial flux switched-reluctance motor," in *Proc. IEEE Int. Conf. Electric Mach. Drives*, May 2005, pp. 1130–1134.
[5] C.-T. Liu and T.-S. Chiang, "Design and performance evaluation of a microlinear switched-reluctance motor," *IEEE Trans. Magn.*, vol. 40, no. 2, pp. 806–809, Mar. 2004, doi: 10.1109/TMAG.2004.824560.
[6] B. Bilgin, J. W. Jiang, and A. Emadi, *Switched Reluctance Motor Drives Fundamentals to Applications*. Boca Raton, FL, USA: CRC Press, 2019.
[7] R. Vandana and B. G. Fernandes, "Design methodology for high-performance segmented rotor switched reluctance motors," *IEEE Trans. Energy Convers.*, vol. 30, no. 1, pp. 11–21, Mar. 2015, doi: 10.1109/TEC.2014.2336861.
[8] H. Torkaman, N. Faraji, and M. S. Toulabi, "Influence of rotor structure on fault diagnosis indices in two-phase switched reluctance motors," *IEEE Trans. Magn.*, vol. 50, no. 3, pp. 136–143, Mar. 2014, doi: 10.1109/TMAG.2013.2285882.
[9] M. Asgar, E. Afjei, and H. Torkaman, "A new strategy for design and analysis of a double-stator switched reluctance motor: Electromagnetics, FEM, and experiment," *IEEE Trans. Magn.*, vol. 51, no. 12, pp. 1–8, Aug. 2015, doi: 10.1109/TMAG.2015.2465307.
[10] Y. Hu, C. Gan, W. Cao, J. Zhang, W. Li, and S. J. Finney, "Flexible fault-tolerant topology for switched reluctance motor drives," *IEEE Trans. Power Electron.*, vol. 31, no. 6, pp. 4654–4668, Jun. 2016, doi: 10.1109/TPEL.2015.2477165.
[11] J. W. Jiang, B. Bilgin, and A. Emadi, "Three-phase 24/16 switched reluctance machine for a hybrid electric powertrain," *IEEE Trans. Transport. Electrific.*, vol. 3, no. 1, pp. 76–85, Mar. 2017, doi: 10.1109/TTE.2017.2664778.
[12] E. Bostanci, M. Moallem, A. Parsapour, and B. Fahimi, "Opportunities and challenges of switched reluctance motor drives for electric propulsion: A comparative study," *IEEE Trans. Transport. Electrific.*, vol. 3, no. 1, pp. 58–75, Mar. 2017, doi: 10.1109/TTE.2017.2649883.
[13] J. Lin, N. Schofield, and A. Emadi, "External-rotor 6-10 switched reluctance motor for an electric bicycle," *IEEE Trans. Transport. Electrific.*, vol. 1, no. 4, pp. 348–356, Dec. 2015, doi: 10.1109/TTE.2015.2502543.
[14] H. Zhang, W. Xu, S. Wang, Y. Huangfu, G. Wang, and J. Zhu, "Optimum design of rotor for high-speed switched reluctance motor using level set method," *IEEE Trans. Magn.*, vol. 50, no. 2, pp. 765–768, Feb. 2014, doi: 10.1109/TMAG.2013.2285393.
[15] E. Afjei, A. Siadatan, and H. Torkaman, "Magnetic modeling, prototyping, and comparative study of a quintuple-set switched reluctance motor," *IEEE Trans. Magn.*, vol. 51, no. 8, pp. 1–7, Aug. 2015, doi: 10.1109/TMAG.2015.2418257.
[16] M. M. Nezamabadi, E. Afjei, and H. Torkaman, "Design, dynamic electromagnetic analysis, FEM, and fabrication of a new switched-reluctance motor with hybrid motion," *IEEE Trans. Magn.*, vol. 52, no. 4, pp. 1–8, Apr. 2016, doi: 10.1109/TMAG.2015.2504522.
[17] H. Torkaman and E. Afjei, "Sensorless method for eccentricity fault monitoring and diagnosis in switched reluctance machines based on stator voltage signature," *IEEE Trans. Magn.*, vol. 49, no. 2, pp. 912–920, Feb. 2013.
[18] H. Torkaman, A. Ghaheri, and A. Keyhani, "Axial flux switched reluctance machines: A comprehensive review of design and topologies," *IET Electr. Power Appl.*, vol. 13, no. 3, pp. 310–321, Mar. 2019, doi: 10.1049/iet-epa.2018.5190.
[19] B. G. Joseph and P. C. Thomas, "Variable reluctance axial flux alternator incorporating air gap variation," in *Proc. Biennial Int. Conf. Power Energy Syst., Towards Sustain. Energy (PESTSE)*, Jan. 2016, pp. 1–8.
[20] N. K. Sheth and K. R. Rajagopal, "Effects of nonuniform airgap on the torque characteristics of a switched reluctance motor," *IEEE Trans. Magn.*, vol. 40, no. 4, pp. 2032–2034, Jul. 2004, doi: 10.1109/TMAG.2004.832173.

[21] B. Bilgin, B. Howey, A. D. Callegaro, J. Liang, M. Kordic, J. Taylor, and A. Emadi, "Making the case for switched reluctance motors for propulsion applications," *IEEE Trans. Veh. Technol.*, vol. 69, no. 7, pp. 7172–7186, Jul. 2020, doi: 10.1109/TVT.2020.2993725.

[22] M. Howell. (2020). *Switched Reluctance Motor*. [Online]. Available: https://www.easa.com

[23] R. Vandana, S. Nikam, and B. G. Fernandes, "Criteria for design of high performance switched reluctance motor," in *Proc. 20th Int. Conf. Electr. Mach.*, Sep. 2012, pp. 129–135.

[24] B. Bilgin, A. Emadi, and M. Krishnamurthy, "Design considerations for switched reluctance machines with a higher number of rotor poles," *IEEE Trans. Ind. Electron.*, vol. 59, no. 10, pp. 3745–3756, Oct. 2012, doi: 10.1109/TIE.2011.2141102.

[25] P. C. Desai, M. Krishnamurthy, N. Schofield, and A. Emadi, "Novel switched reluctance machine configuration with higher number of rotor poles than stator poles: Concept to implementation," *IEEE Trans. Ind. Electron.*, vol. 57, no. 2, pp. 649–659, Feb. 2010, doi: 10.1109/TIE.2009.2034678.

[26] J. D. Widmer and B. C. Mecrow, "Optimised segmental rotor switched reluctance machines with a greater number of rotor segments than stator slots," in *Proc. IEEE Int. Electr. Mach. Drives Conf. (IEMDC)*, May 2011, pp. 1183–1188.

[27] V. Rallabandi and B. G. Fernandes, "Design procedure of segmented rotor switched reluctance motor for direct drive applications," *IET Electr. Power Appl.*, vol. 8, no. 3, pp. 77–88, Mar. 2014, doi: 10.1049/iet-epa.2013.0154.

[28] T. J. E. Miller, "Converter volt-ampere requirements of the switched reluctance motor drive," *IEEE Trans. Ind. Appl.*, vol. IA-21, no. 5, pp. 1136–1144, Sep. 1985, doi: 10.1109/TIA.1985.349516.

[29] J. Zhu, K. W. E. Cheng, and X. Xue, "Torque analysis for in-wheel switched reluctance motors with varied number of rotor poles," in *Proc. Int. Symp. Electr. Eng. (ISEE)*, Dec. 2016, pp. 1–5.

[30] B. Wang, D.-H. Lee, C.-W. Lee, and J.-W. Ahn, "Characteristics analysis of a novel segmental rotor axial field switched reluctance motor with single teeth winding," *J. Power Electron.*, vol. 14, no. 5, pp. 852–858, Sep. 2014, doi: 10.6113/JPE.2014.14.5.852.

[31] D.-C. Pang and C.-T. Wang, "A wireless-driven, micro, axial-flux, single-phase switched reluctance motor," *Energies*, vol. 11, no. 10, p. 2772, Oct. 2018. 10.3390/en11102772.

[32] F. Sass, J. A. Santisteban, and E. Sanches, "Design and implementation of a digital control system for an axial flux switched reluctance motor," in *Proc. Brazilian Power Electron. Conf.*, Sep. 2009, pp. 138–144.

[33] H. Arihara and K. Akatsu, "A basic property of axial type switched reluctance motor," in *Proc. Int. Conf. Electr. Mach. Syst.*, 2010, pp. 1687–1690.

[34] T. Kellerer and O. Radler, "Axial type switched reluctance motor of soft magnetic composite," in *Proc. Innov. Small Drives Micro-Motor Syst., GMM/ETG Symp.*, 2013, pp. 1–6.

[35] J. Ma, R. Qu, and J. Li, "Optimal design of axial flux switched reluctance motor for electric vehicle application," in *Proc. 17th Int. Conf. Electr. Mach. Syst. (ICEMS)*, Oct. 2014, pp. 1860–1865.

[36] J. Ma, R. Qu, and J. Li, "A novel axial flux switched reluctance motor with grain oriented electrical steel," in *Proc. IEEE Magn. Conf. (INTERMAG)*, May 2015, p. 1.

[37] D. W. J. Pulle and I. R. Petersen, "A unified approach to switched reluctance drive modeling: Application to an axial flux (SRAF) motor," in *Proc. Power Electron. Spec. Conf., PESC Rec. 29th Annual IEEE*, vol. 2, May 1998, pp. 1681–1686.

[38] B.-S. Lee, H.-K. Bae, P. Vijayraghavan, and R. Krishnan, "Design of a linear switched reluctance machine," *IEEE Trans. Ind. Appl.*, vol. 36, no. 6, pp. 1571–1580, Nov. 2000, doi: 10.1109/28.887208.

[39] H. Chen, R. Nie, and W. Yan, "A novel structure single-phase tubular switched reluctance linear motor," *IEEE Trans. Magn.*, vol. 53, no. 11, pp. 1–4, Nov. 2017, doi: 10.1109/TMAG.2017.2700007.

[40] H. Chen, R. Nie, and Q. Wang, "Unbalanced normal force reduction in the eccentric double-sided linear switched reluctance machine," *IET Electr. Power Appl.*, vol. 10, no. 5, pp. 384–393, May 2016, doi: 10.1049/iet-epa.2015.0419.

[41] J. F. Pan, N. C. Cheung, and Y. Zou, "Design and analysis of a novel transverse-flux tubular linear machine with gear-shaped teeth structure," *IEEE Trans. Magn.*, vol. 48, no. 11, pp. 3339–3343, Nov. 2012, doi: 10.1109/TMAG.2012.2202377.

[42] L. Yan, W. Li, Z. Jiao, and I.-M. Chen, "Novel tubular switched reluctance motor with double excitation windings: Design, modeling, and experiments," *Rev. Sci. Instrum.*, vol. 86, no. 12, Dec. 2015, Art. no. 125004.

[43] X. Xue, K. W. E. Cheng, and Z. Zhang, "Model, analysis, and application of tubular linear switched reluctance actuator for linear compressors," *IEEE Trans. Ind. Electron.*, vol. 65, no. 12, pp. 9863–9872, Dec. 2018, doi: 10.1109/TIE.2018.2818638.

[44] M. T. Khor, R. Sotudeh, and D. Lee, "Switched reluctance motor based on short flux path control method," in *Proc. 39th Int. Universities Power Eng. Conf.*, Sep. 2004, pp. 559–562.

[45] X. Zhang, L. Xiong, and M. Zhang, "The research on an inter-phase coupling switched reluctance motor with short flux path," in *Proc. IEEE 4th Adv. Inf. Technol., Electron. Automat. Control Conf. (IAEAC)*, Dec. 2019, pp. 490–493.

[46] H. Hwang, J. Hur, and C. Lee, "Novel permanent-magnet-assisted switched reluctance motor (I): Concept, design, and analysis," in *Proc. Int. Conf. Electr. Mach. Syst. (ICEMS)*, Oct. 2013, pp. 602–608.

[47] J. Jeong, J. Her, and C. Lee, "Novel permanent-magnet-assisted switched reluctance motor (II): Concept, design, and analysis," in *Proc. Int. Conf. Electr. Mach. Syst. (ICEMS)*, Oct. 2013, pp. 609–614.

[48] M. Vosswinkel, A. Lohner, V. Platte, and T. Hirche, "Design, production, and verification of a switched-reluctance wheel hub drive train for battery electric vehicles," *World Electr. Vehicle J.*, vol. 10, no. 4, p. 82, Nov. 2019.

[49] V. Hanaeinejad and M. Abbasian, "A non-segmental outer rotor switched reluctance machine for in-wheel electric vehicle application," *Iranian J. Sci. Technol., Trans. Electr. Eng.*, vol. 43, no. 4, pp. 909–918, Dec. 2019, doi: 10.1007/s40998-019-00192-9.

[50] M. Cinar and F. Erfan Kuyumcu, "Design and torque profile analysis of an outer-rotor SR motor with different winding configurations," *Przegląd Elektrotechniczny*, vol. 88, no. 2, pp. 328–331, 2012.

[51] N. Arbab, H. Karim, and H. Torkaman, "New external rotor switched reluctance motor in comparison with conventional SRM," *IREE Int. Rev. Electr. Eng.*, vol. 6, no. 2, pp. 679–684, Mar. 2011.

[52] M. A. Kabir and I. Husain, "Concentrated winding segmented rotor switched reluctance machine (SRM) using three-phase standard inverters," in *Proc. IEEE Energy Convers. Congr. Expo. (ECCE)*, Sep. 2015, pp. 5567–5572.

[53] W. Bo, D.-H. Lee, and J.-W. Ahn, "A novel axial field SRM with segmental rotor: Concept, design and analysis," in *Proc. Workshop Power Electron. Power Quality Appl. (PEPQA)*, Jul. 2013.

[54] T. Shibamoto, K. Nakamura, H. Goto, and O. Ichinokura, "A design of axial-gap switched reluctance motor for in-wheel direct-drive EV," in *Proc. 20th Int. Conf. Electr. Mach.*, Sep. 2012, pp. 1160–1165.

[55] R. Madhavan and B. G. Fernandes, "A novel axial flux segmented SRM for electric vehicle application," in *Proc. 19th Int. Conf. Electr. Mach. (ICEM)*, Sep. 2010, pp. 0–5.

[56] R. Madhavan and B. G. Fernandes, "Comparative analysis of axial flux SRM topologies for electric vehicle application," in *Proc. IEEE Int. Conf. Power Electron., Drives Energy Syst. (PEDES)*, Dec. 2012, pp. 1–6.

[57] H. Goto, S. Murakami, and O. Ichinokura, "Design to maximize torque-volume density of axial-flux SRM for in-wheel EV," in *Proc. 41st Annu. Conf. IEEE Ind. Electron. Soc. (IECON)*, Nov. 2015, pp. 5191–5196.

[58] M. Sengupta, S. S. Ahmad, and D. Mukherjee, "Experimental investigations on a novel laboratory prototype of axial flux switched reluctance motor," in *Proc. IEEE Int. Conf. Power Electron., Drives Energy Syst.*, Dec. 2012, pp. 1–5.

[59] F. Daldaban and N. Ustkoyuncu, "New disc type switched reluctance motor for high torque density," *Energy Convers. Manage.*, vol. 48, no. 8, pp. 2424–2431, Aug. 2007.

[60] D. Wang, C. Shao, and X. Wang, "Design and performance evaluation of a tubular linear switched reluctance generator with low cost and high thrust density," *IEEE Trans. Appl. Supercond.*, vol. 26, no. 7, pp. 1–5, Oct. 2016.

[61] D. Wang, C. Shao, and X. Wang, "Design and performance evaluation of a tubular linear switched reluctance generator with low cost and high thrust density," *IEEE Trans. Appl. Supercond.*, vol. 26, no. 7, pp. 1–5, Oct. 2016, doi: 10.1109/TASC.2016.2599202.

[62] W. Li, C.-Y. Chen, L. Yan, Z. Jiao, and I.-M. Chen, "Design and modeling of tubular double excitation windings linear switched reluctance motor," in *Proc. IEEE 10th Conf. Ind. Electron. Appl. (ICIEA)*, Jun. 2015, pp. 1686–1691.

[63] E. Sayed, M. H. Bakr, B. Bilgin, and A. Emadi, "Gradient-based design optimization of a switched reluctance motor for an HVAC application," in *Proc. IEEE Transp. Electrific. Conf. Expo (ITEC)*, Jun. 2020, pp. 1031–1037, doi: 10.1109/ITEC48692.2020.9161741.

[64] D. Jonathan, D. Bruno, and B. A. Hamid, "Simulated annealing and genetic algorithms in topology optimization tools: A comparison through the design of a switched reluctance machine," in *Proc. SPEEDAM*, Jun. 2010, pp. 1247–1252.

[65] H. Li, B. Bilgin, and A. Emadi, "An improved torque sharing function for torque ripple reduction in switched reluctance machines," *IEEE Trans. Power Electron.*, vol. 34, no. 2, pp. 1635–1644, Feb. 2019, doi: 10.1109/TPEL.2018.2835773.

[66] S. Li, S. Zhang, T. G. Habetler, and R. G. Harley, "Modeling, design optimization, and applications of switched reluctance machines—A review," *IEEE Trans. Ind. Appl.*, vol. 55, no. 3, pp. 2660–2681, May 2019, doi: 10.1109/TIA.2019.2897965.

[67] Y. Yasa, Y. Sozer, and M. Garip, "High-power density switched reluctance machine development for high-speed spindle applications," *Turkish J. Electr. Eng. Comput. Sci.*, vol. 26, no. 3, pp. 1572–1586, May 2018, doi: 10.3906/elk-1706-288.

[68] H. Hayashi, K. Nakamura, A. Chiba, T. Fukao, K. Tungpimolrut, and D. G. Dorrell, "Efficiency improvements of switched reluctance motors with high-quality iron steel and enhanced conductor slot fill," *IEEE Trans. Energy Convers.*, vol. 24, no. 4, pp. 819–825, Dec. 2009, doi: 10.1109/TEC.2009.2025425.

[69] Y. Takano, A. Chiba, S. Ogasawara, M. Takeno, N. Hoshi, T. Imakawa, and M. Takemoto, "Torque density and efficiency improvements of a switched reluctance motor without rare Earth material for hybrid vehicles," in *Proc. IEEE Energy Convers. Congr. Expo.*, Sep. 2010, pp. 2653–2659.

[70] M. Morimoto, "Efficiency improvement of induction motor by 3-D core made of SMC," in *Proc. 15th Int. Power Electron. Motion Control Conf. (EPE/PEMC)*, Sep. 2012, pp. LS1b.3-1–LS1b.3-5.

[71] C. Lin and B. Fahimi, "Prediction of acoustic noise in switched reluctance motor drives," *IEEE Trans. Energy Convers.*, vol. 29, no. 1, pp. 250–258, Mar. 2014, doi: 10.1109/TEC.2013.2291702.

[72] M. Elamin, "Acoustic nosie mitigation of switched reluctance machines through skewing methods," M.S. thesis, Univ. Akron, OH, USA, 2017.

[73] D. Tekgun, "Acoustic noise and vibration reduction on switched reluctance machines through hole placement in stator/rotor laminations," M.S. thesis, Univ. Akron, OH, USA, 2017.

[74] O. Gundogmus, L. Vadamodala, Y. Sezer, J. Kutz, J. Tylenda, and R. L. Wright, "Simultaneous torque and radial force ripple mitigation in DQ controlled switched reluctance machines," in *Proc. IEEE Int. Electric Mach. Drives Conf. (IEMDC)*, May 2019, pp. 260–265.

[75] J. Dong, J. W. Jiang, B. Howey, H. Li, B. Bilgin, A. D. Callegaro, and A. Emadi, "Hybrid acoustic noise analysis approach of conventional and mutually coupled switched reluctance motors," *IEEE Trans. Energy Convers.*, vol. 32, no. 3, pp. 1042–1051, Sep. 2017.

[76] A. D. Callegaro, J. Liang, J. W. Jiang, B. Bilgin, and A. Emadi, "Radial force density analysis of switched reluctance machines: The source of acoustic noise," *IEEE Trans. Transport. Electrific.*, vol. 5, no. 1, pp. 93–106, Mar. 2019, doi: 10.1109/TTE.2018.2887338.

[77] M. Abdalmagid, M. Bakr, E. Sayed, and A. Emadi, "Adjoint sensitivity analysis of radial force components of switched reluctance machines," in *Proc. IEEE Transp. Electrific. Conf. Expo (ITEC)*, Jun. 2021, pp. 395–400.

[78] S. Hosseini and Y. Alinejad-Beromi, "Noise reduction in switched reluctance motor by modifying the structures," *IET Electr. Power Appl.*, vol. 14, no. 14, pp. 2863–2872, Dec. 2020, doi: 10.1049/iet-epa.2020.0081.

[79] A. D. Callegaro, B. Bilgin, and A. Emadi, "Radial force shaping for acoustic noise reduction in switched reluctance machines," *IEEE Trans. Power Electron.*, vol. 34, no. 10, pp. 9866–9878, Oct. 2019, doi: 10.1109/TPEL.2019.2891050.

[80] J. Furqani, M. Kawa, K. Kiyota, and A. Chiba, "Comparison of current waveforms for noise reduction in switched reluctance motors," in *Proc. IEEE Energy Convers. Congr. Expo. (ECCE)*, Oct. 2017, pp. 752–759.

[81] J. Y. Chai, Y. W. Lin, and C. M. Liaw, "Comparative study of switching controls in vibration and acoustic noise reductions for switched reluctance motor," *IEE Proc. Electr. Power Appl.*, vol. 153, no. 3, p. 348, 2006, doi: 10.1049/ip-epa:20050340.

[82] C. Ma, L. Qu, R. Mitra, P. Pramod, and R. Islam, "Vibration and torque ripple reduction of switched reluctance motors through current profile optimization," in *Proc. IEEE Appl. Power Electron. Conf. Expo. (APEC)*, Mar. 2016, pp. 3279–3285.

[83] M. Cavazzuti, *Optimization Methods: From Theory to Design, Scientific and Technological Aspects in Mechanics*, 1st ed. Berlin, Germany: Springer, 2013.

[84] M. H. Bakr, *Nonlinear Optimization in Electrical Engineering with Applications in MATLAB*. Edison, NJ, USA: IET, 2013.

[85] D. M. Kulkarni, "Continuum sensitivity analysis using boundary velocity formulation for shape derivatives," Ph.D. dissertation, Virginia Polytech. Inst. State Univ., USA, 2016.

[86] E. Sayedm, "Adjoint-based optimization of switched reluctance motors," Ph.D. dissertation, Mcmaster Univ., ON, Canada, 2019.

[87] L. S. Kalantari, O. Ahmed, M. H. Bakr, and N. K. Nikolova, "Adjoint sensitivity analysis of 3D problems with anisotropic materials," in *IEEE MTT-S Int. Microw. Symp. Dig.*, Jun. 2014, pp. 1–3.

[88] Y. Zhang, O. S. Ahmed, and M. H. Bakr, "Adjoint sensitivity analysis of plasmonic structures using the FDTD method," *Opt. Lett.*, vol. 39, no. 10, pp. 3002–3005, 2014.

[89] G. Dziatkiewicz, "Complex variable step method for sensitivity analysis of effective properties in multi-field micromechanics," *Acta Mechanica*, vol. 227, no. 1, pp. 11–28, Jan. 2016, doi: 10.1007/s00707-015-1419-y.

[90] K.-L. Lai and J. L. Crassidis, "Extensions of the first and second complex-step derivative approximations," *J. Comput. Appl. Math.*, vol. 219, no. 1, pp. 276–293, Sep. 2008, doi: 10.1016/j.cam.2007.07.026.

[91] E. Sayed, M. H. Bakr, B. Bilgin, and A. Emadi, "A MATLAB toolbox for adjoint-based sensitivity analysis of switched reluctance motors," in *Proc. IEEE Electr. Power Energy Conf. (EPEC)*, Oct. 2018, pp. 2018–2021.

[92] S.-B. Park, H.-B. Lee, S.-Y. Hahn, and I.-H. Park, "Stator slot shape design of induction motors for iron loss reduction," *IEEE Trans. Magn.*, vol. 31, no. 3, pp. 2004–2007, May 1995, doi: 10.1109/20.376436.

[93] S.-H. Lee, D.-H. Kim, J.-H. Lee, B.-S. Kim, and I.-H. Park, "Shape design sensitivity for force density distribution of magnetic systems," *IEEE Trans. Appl. Supercond.*, vol. 12, no. 1, pp. 1471–1474, Mar. 2002, doi: 10.1109/TASC.2002.1018680.

[94] K. H. Lee, S. G. Hong, M. K. Baek, H. S. Choi, Y. S. Kim, and I. H. Park, "Adaptive level set method for accurate boundary shape in optimization of electromagnetic systems," *COMPEL Int. J. Comput. Math. Electr. Electron. Eng.*, vol. 33, no. 3, pp. 809–820, Apr. 2014, doi: 10.1108/COMPEL-10-2012-0218.

[95] K. H. Lee, C. Y. Choi, and I. H. Park, "Continuum sensitivity analysis and shape optimization of Dirichlet conductor boundary in electrostatic system," *IEEE Trans. Magn.*, vol. 54, no. 3, pp. 1–4, Mar. 2018, doi: 10.1109/TMAG.2017.2758202.

[96] I.-H. Park, J.-L. Coulomb, and S.-Y. Hahn, "Implementation of continuum sensitivity analysis with existing finite element code," *IEEE Trans. Magn.*, vol. 29, no. 2, pp. 1787–1790, Mar. 1993, doi: 10.1109/20.250752.

[97] E. Kuci, F. Henrotte, P. Duysinx, P. Dular, and C. Geuzaine, "Design sensitivity analysis for shape optimization of nonlinear magnetostatic systems," *IEEE Trans. Magn.*, vol. 52, no. 3, pp. 1–4, Mar. 2016, doi: 10.1109/TMAG.2015.2478196.

[98] M. H. Bakr, O. S. Ahmed, M. H. El Sherif, and T. Nomura, "Time domain adjoint sensitivity analysis of electromagnetic problems with nonlinear media," *Opt. Exp.*, vol. 22, no. 9, pp. 10831–10843, 2014.

[99] S. Akbarzadeh, J. Hückelheim, and J.-D. Müller, "Consistent treatment of incompletely converged iterative linear solvers in reverse-mode algorithmic differentiation," *Comput. Optim. Appl.*, vol. 77, no. 2, pp. 597–616, Nov. 2020, doi: 10.1007/s10589-020-00214-x.

[100] P. Enciu, F. Wurtz, and L. Gerbaud, "Automatic differentiation for sensitivity calculation in electromagnetism: Application for optimization of a linear actuator," in *Proc. Dig. 14th Biennial IEEE Conf. Electromagn. Field Comput.*, May 2010, p. 1.

[101] W. Rosanisah, W. Mohd, and L. Abdullah, "Aggregation methods in group decision making: A decade survey," *Informatica*, vol. 41, pp. 71–86, Feb. 2017.

[102] C. Sauvey, J.-F. Antoine, C. Visa, and G. Abba, "Optimization of the design for a switched reluctance drive controlled by trapezoidal shaped currents," in *Proc. 44th IEEE Conf. Decis. Control*, Dec. 2005, pp. 3892–3897.

[103] G. Lei, J. Zhu, Y. Guo, C. Liu, and B. Ma, "A review of design optimization methods for electrical machines," *Energies*, vol. 10, no. 12, p. 1962, Nov. 2017.

[104] Y. Goynuk, "Development of an electrical machines analysis and optimum design software package," M.S. thesis, Middle East Tech. Univ., Ankara, Turkey, 2008.

[105] X.-S. Yang, *Engineering Mathematics with Examples and Applications*. London, U.K.: Academic, 2017.

[106] V. Dehdari and D. S. Oliver, "Sequential quadratic programming for solving constrained production optimization–case study from Brugge field," *SPE J.*, vol. 17, no. 3, pp. 874–884, Sep. 2012.

[107] G. Astfalk, I. Lustig, R. Marsten, and D. Shanno, "The interior-point method for linear programming," *IEEE Softw.*, vol. 9, no. 4, pp. 61–68, Jul. 1992.

[108] R. H. W. Hoppe, C. Linsenmann, and S. I. Petrova, "Primal-dual Newton methods in structural optimization," *Comput. Visualizat. Sci.*, vol. 9, no. 2, pp. 71–87, Jun. 2006, doi: 10.1007/s00791-006-0018-9.

[109] D. Den Hertog, *Interior Point Approach to Linear, Quadratic and Convex Programming: Algorithms and Complexity*. Norwell, MA, USA: Kluwer, 1993.

[110] M. Clerc, "Particle swarm optimization," in *IEEE Int. Conf. Neural Netw.*, Nov. 1995, pp. 1942–1948.

[111] W. Hu and G. G. Yen, "Adaptive multiobjective particle swarm optimization based on parallel cell coordinate system," *IEEE Trans. Evol. Comput.*, vol. 19, no. 1, pp. 1–18, Feb. 2015, doi: 10.1109/TEVC.2013.2296151.

[112] C. Ma and L. Qu, "Multiobjective optimization of switched reluctance motors based on design of experiments and particle swarm optimization," *IEEE Trans. Energy Convers.*, vol. 30, no. 3, pp. 1144–1153, Sep. 2015, doi: 10.1109/TEC.2015.2411677.

[113] M. Reyes-Sierra and C. A. Coello, "Multi-objective particle swarm optimizers: A survey of the state-of-the-art," *Int. J. Comput. Intell. Res.*, vol. 2, no. 3, pp. 287–308, 2006.

[114] S. Kirkpatrick, C. D. Gelatt, and M. P. Vecchi, "Optimization by simulated annealing," *Science*, vol. 220, no. 4598, pp. 671–680, 1983, doi: 10.5019/j.ijcir.2006.68.

[115] R. T. Naayagi and V. Kamaraj, "A comparative study of shape optimization of SRM using genetic algorithm and simulated annealing," in *Proc. Annu. IEEE India Conf. (Indicon)*, Dec. 2005, pp. 596–599.

[116] P. Guo, X. Wang, and Y. Han, "The enhanced genetic algorithms for the optimization design," in *Proc. 3rd Int. Conf. Biomed. Eng. Informat.*, Oct. 2010, pp. 2990–2994.

[117] C. W. Ahn, *Advances in Evolutionary Algorithms*. Berlin, Germany: Springer-Verlag, 2006.

[118] M. Potvin and G. Jean-Yves, *Handbook of Metaheuristics*, 2nd ed. New York, NY, USA: Springer, 2010.

[119] B. Wang, "A novel artificial bee colony algorithm based on modified search strategy and generalized opposition-based learning," *J. Intell. Fuzzy Syst.*, vol. 28, no. 3, pp. 1023–1037, 2015, doi: 10.3233/IFS-141386.

[120] F. S. Abu-Mouti and M. E. El-Hawary, "Optimal distributed generation allocation and sizing in distribution systems via artificial bee colony algorithm," *IEEE Trans. Power Del.*, vol. 26, no. 4, pp. 2090–2101, Oct. 2011, doi: 10.23919/ChiCC.2019.8866068.

[121] L. Cheng, M. Yu, J. Yang, and Y. Wang, "An improved artificial BEE colony algorithm based on beetle antennae search," in *Proc. Chin. Control Conf. (CCC)*, Jul. 2019, pp. 2312–2316.

[122] I. Aljarah and S. A. Ludwig, "A new clustering approach based on glowworm swarm optimization," in *Proc. IEEE Congr. Evol. Comput.*, Jun. 2013, pp. 2642–2649.

[123] H. Deng-Xu, L. Gui-Qing, and Z. Hua-Zheng, "Glowworm swarm optimization algorithm for solving multi-objective optimization problem," in *Proc. 9th Int. Conf. Comput. Intell. Secur.*, Dec. 2013, pp. 11–15.

[124] M. Alb, P. Alotto, C. Magele, W. Renhart, K. Preis, and B. Trapp, "Firefly algorithm for finding optimal shapes of electromagnetic devices," *IEEE Trans. Magn.*, vol. 52, no. 3, pp. 1–4, Mar. 2016, doi: 10.1109/TMAG.2015.2483058.

[125] A. Ritthipakdee, A. Thammano, N. Premasathian, and D. Jitkongchuen, "Firefly mating algorithm for continuous optimization problems," *Comput. Intell. Neurosci.*, vol. 2017, pp. 1–10, Jul. 2017.

[126] X. S. Yang and S. Deb, "Cuckoo search via Lèvy flights," in *Proc. World Congr. Nat. Biol. Inspired Comput. (NABIC)*, 2009, pp. 210–214.

[127] T. C. Bora, L. D. S. Coelho, and L. Lebensztajn, "Bat-inspired optimization approach for the brushless DC wheel motor problem," *IEEE Trans. Magn.*, vol. 48, no. 2, pp. 947–950, Feb. 2012, doi: 10.1109/TMAG.2011.2176108.

[128] R. Oftadeh and M. J. Mahjoob, "A new meta-heuristic optimization algorithm: Hunting search," in *Proc. 5th Int. Conf. Soft Comput., Comput. Words Perceptions Syst. Anal., Decis. Control*, Sep. 2009.

[129] I.-S. Yang, R. Xiao, M. Karamanoglu, Z. Cui, and A. H. Gandomi, *Swarm Intelligence and Bio-Inspired Computation*. London, U.K.: Elsevier, 2013.

[130] D. Fodorean, L. Idoumghar, A. N'Diaye, D. Bouquain, and A. Miraoui, "Simulated annealing algorithm for the optimisation of an electrical machine," *IET Electr. Power Appl.*, vol. 6, no. 9, pp. 735–742, Nov. 2012, doi: 10.1049/iet-epa.2011.0029.

[131] A.-H. Zhou, L.-P. Zhu, B. Hu, S. Deng, Y. Song, H. Qiu, and S. Pan, "Traveling-salesman-problem algorithm based on simulated annealing and gene-expression programming," *Information*, vol. 10, no. 1, p. 7, Dec. 2018, doi: 10.3390/info10010007.

[132] X. Dong, D. Ouyang, D. Cai, Y. Zhang, and Y. Ye, "A hybrid discrete PSO-SA algorithm to find optimal elimination orderings for Bayesian networks," in *Proc. 2nd Int. Conf. Ind. Inf. Syst.*, Jul. 2010, pp. 510–513.

[133] R. L. Haupt, "An introduction to genetic algorithms for electromagnetics," *IEEE Antennas Propag. Mag.*, vol. 37, no. 2, pp. 7–15, Apr. 1995, doi: 10.1109/74.382334.

[134] A. Plerou, E. Vlamou, and V. Papadopoulos, "Fuzzy genetic algorithms: Fuzzy logic controllers and genetics algorithms," *Glob. J. Res. Anal.*, vol. 5, no. 11, pp. 497–500, 2016.

[135] M. Vannucci, V. Colla, S. Dettori, and V. Iannino, "Fuzzy adaptive genetic algorithm for improving the solution of industrial optimization problems," *J. Intell. Syst.*, vol. 29, no. 1, pp. 409–422, Feb. 2018, doi: 10.1515/jisys-2016-0343.

[136] B. Mirzaeian, M. Moallem, V. Tahani, and C. Lucas, "Multiobjective optimization method based on a genetic algorithm for switched reluctance motor design," *IEEE Trans. Magn.*, vol. 38, no. 3, pp. 1524–1527, May 2002, doi: 10.1109/20.999126.

[137] A. R. Conn, N. Gould, and P. L. Toint, "A globally convergent Lagrangian barrier algorithm for optimization with general inequality constraints and simple bounds," *Math. Comput.*, vol. 66, no. 217, pp. 261–289, Jan. 1997.

[138] J.-Y. Lee, J.-H. Chang, D.-H. Kang, S.-I. Kim, and J.-P. Hong, "Tooth shape optimization for cogging torque reduction of transverse flux rotary motor using design of experiment and response surface methodology," *IEEE Trans. Magn.*, vol. 43, no. 4, pp. 1817–1820, Apr. 2007, doi: 10.1109/TMAG.2007.892611.

[139] G. Wang, "Adaptive response surface method using inherited Latin hypercube design points," *J. Mech. Des.*, vol. 125, no. 2, pp. 210–220, Jun. 2003, doi: 10.1115/1.1561044.

[140] C. Huang and G. Yang, "Optimization design of switched reluctance motor based on response surface method," in *Proc. IEEE Student Conf. Electr. Mach. Syst.*, Dec. 2018, pp. 1–6.

[141] R. T. Ogulata and S. M. Mezarcioz, "Optimization of air permeability of knitted fabrics with the Taguchi approach," *J. Textile Inst.*, vol. 102, no. 5, pp. 395–404, May 2011.

[142] Y. Gong, S. Zhao, and S. Luo, "Design and optimization of switched reluctance motor by Taguchi method," in *Proc. 13th IEEE Conf. Ind. Electron. Appl. (ICIEA)*, May 2018, pp. 1876–1880.

[143] K. Diao, X. Sun, G. Lei, G. Bramerdorfer, Y. Guo, and J. Zhu, "Robust design optimization of switched reluctance motor drive systems based on system-level sequential Taguchi method," *IEEE Trans. Energy Convers.*, vol. 36, no. 4, pp. 3199–3207, Dec. 2021, doi: 10.1109/TEC.2021.3085668.

[144] W. Yan, H. Chen, X. Liu, X. Ma, Z. Lv, X. Wang, R. Palka, L. Chen, and K. Wang, "Design and multi-objective optimisation of switched reluctance machine with iron loss," *IET Electr. Power Appl.*, vol. 13, no. 4, pp. 435–444, Apr. 2019, doi: 10.1049/iet-epa.2018.5699.

[145] M. Afifi, H. Rezk, M. Ibrahim, and M. El-Nemr, "Multi-objective optimization of switched reluctance machine design using Jaya algorithm (MO-Jaya)," *Mathematics*, vol. 9, no. 10, p. 1107, May 2021, doi: 10.3390/math9101107.

[146] X. Gao, R. Na, C. Jia, X. Wang, and Y. Zhou, "Multi- objective optimization of switched reluctance motor drive in electric vehicles," *Comput. Electr. Eng.*, vol. 70, pp. 914–930, Aug. 2018, doi: 10.1016/j.compeleceng.2017.12.016.

[147] O. B. Augusto, F. Bennis, and S. Caro, "A new method for decision making in multi-objective optimization problems," *Pesquisa Operacional*, vol. 32, no. 2, pp. 331–369, Jun. 2012, doi: 10.1590/S0101-74382012005000014.
[148] A. Bentounsi, F. Rebahi, and R. E. H. Bouchekara, "Multi-objective optimization design of 8/6 switched reluctance motor using GA and PSO algorithms," *J. Electr. Eng. Technol.*, vol. 15, no. 4, pp. 168–175, 2015.
[149] R. T. Naayagi and V. Kamaraj, "Shape optimization of switched reluctance machine for aerospace applications," in *Proc. 31st Annu. Conf. IEEE Ind. Electron. Soc. (IECON)*, Nov. 2005, pp. 1748–1751.
[150] M. Belhadi, G. Krebs, C. Marchand, H. Hannoun, and X. Mininger, "Geometrical optimization of SRM on operating mode for automotive application," *Electr. Eng.*, vol. 100, no. 1, pp. 303–310, Mar. 2018, doi: 10.1007/s00202-016-0504-0.
[151] J. Zhang, H. Wang, L. Chen, C. Tan, and Y. Wang, "Multi-objective optimal design of bearingless switched reluctance motor based on Multi-objective genetic particle swarm optimizer," *IEEE Trans. Magn.*, vol. 54, no. 1, pp. 1–13, Jan. 2018, doi: 10.1109/TMAG.2017.2751546.
[152] J. Gao, H. Sun, L. He, Y. Dong, and Y. Zheng, "Optimization design of switched reluctance motor based on particle swarm optimization," in *Proc. Int. Conf. Electr. Mach. Syst.*, Aug. 2011, pp. 1–5.
[153] X. D. Xue, K. W. E. Cheng, T. W. Ng, and N. C. Cheung, "Multi-objective optimization design of in-wheel switched reluctance motors in electric vehicles," *IEEE Trans. Ind. Electron.*, vol. 57, no. 9, pp. 2980–2987, Sep. 2010, doi: 10.1109/TIE.2010.2051390.
[154] J. Gao, H. Sun, L. He, Y. Dong, and Y. Zheng, "Optimization design of switched reluctance motor based on particle swarm optimization," in *Proc. Int. Conf. Electr. Mach. Syst. (ICEMS)*, Aug. 2011, pp. 1–5.
[155] M. Balaji and V. Kamaraj, "Particle swarm optimization approach for optimal design of switched reluctance machine," *Amer. J. Appl. Sci.*, vol. 8, no. 4, pp. 374–381, Apr. 2011.
[156] M. Balaji and V. Kamaraj, "Design optimization of switched reluctance machine using particle swarm optimization," in *Proc. 1st Int. Conf. Electr. Energy Syst.*, Jan. 2011, pp. 164–169.
[157] A. S. Oshaba, E. S. Ali, and S. M. A. Elazim, "Speed control of SRM supplied by photovoltaic system via ant colony optimization algorithm," *Neural Comput. Appl.*, vol. 28, no. 2, pp. 365–374, Feb. 2017.
[158] H. Torkaman, E. Afjei, H. Babaee, and P. Yadegari, "Novel method of ACO and its application to rotor position estimation in a SRM under normal and faulty conditions," *J. Power Electron.*, vol. 11, no. 6, pp. 856–863, Nov. 2011, doi: 10.6113/JPE.2011.11.6.856.
[159] M. Yaich and M. Ghariani, "Metaheuristic design and optimization of fuzzy-based SRM speed controller using ant colony algorithm," *J. Eng. Appl. Sci.*, vol. 12, pp. 2782–27388, Oct. 2017, doi: 10.1016/j.neucom.2016.02.076.
[160] J. Evangeline S, S. Suresh Kumar, and J. Jayakumar, "Torque modeling of switched reluctance motor using LSSVM-DE," *Neurocomputing*, vol. 211, pp. 117–128, Oct. 2016.
[161] J. Liu, L. Wang, L. Yi, G. Zhu, and X. Yin, "Optimization of SRM direct instantaneous torque control strategy based on improved firefly algorithm," in *Proc. IEEE 3rd Conf. Energy Internet Energy Syst. Integr. (EI)*, Nov. 2019, pp. 364–368.
[162] A. Yildiz, M. Polat, and M. T. Ozdemir, "Design optimization of inverted switched reluctance motor using ant colony optimization algorithm," in *Proc. Int. Conf. Artif. Intell. Data Process. (IDAP)*, Sep. 2018, pp. 13–18.
[163] B. Laporte, G. Vinsard, and S. Dufour, "Generating rotor geometries by using a genetic method," *IEEE Trans. Magn.*, vol. 36, no. 4, pp. 1039–1042, Jul. 2000.
[164] L. Moreau, M. E. Zaim, and M. Machmoum, "Electromagnetic design optimization of a low speed slotted switched reluctance machine using genetic algorithm," in *Proc. 20th Int. Conf. Electr. Mach.*, Sep. 2012, pp. 233–237.
[165] S. Owatchaiphong, C. Carstensen, and R. W. De Doncker, "Optimization of predesign of switched reluctance machines cross section using genetic algorithms," in *Proc. 7th Int. Conf. Power Electron. Drive Syst.*, Nov. 2007, pp. 707–711.
[166] S. Smaka, S. Konjicija, S. Masic, and M. Cosovic, "Multi-objective design optimization of 8/14 switched reluctance motor," in *Proc. Int. Electr. Mach. Drives Conf.*, May 2013, pp. 468–475.
[167] S. I. Nabeta, I. E. Chabu, L. Lebensztajn, D. A. P. Correa, W. M. D. Silva, and K. Hameyer, "Mitigation of the torque ripple of a switched reluctance motor through a multiobjective optimization," *IEEE Trans. Magn.*, vol. 44, no. 6, pp. 1018–1021, Jun. 2008, doi: 10.1109/TMAG.2007.915137.
[168] X. Cui, J. Sun, C. Gan, C. Gu, and Z. Zhang, "Optimal design of saturated switched reluctance machine for low speed electric vehicles by subset quasi-orthogonal algorithm," *IEEE Access*, vol. 7, pp. 101086–101095, 2019, doi: 10.1109/ACCESS.2019.2929103.
[169] E. Oksuztepe, "In-wheel switched reluctance motor design for electric vehicles by using a Pareto-based multiobjective differential evolution algorithm," *IEEE Trans. Veh. Technol.*, vol. 66, no. 6, pp. 4706–4715, Jun. 2017, doi: 10.1109/TVT.2016.2618119.
[170] E. Sayed, M. H. Bakr, B. Bilgin, and A. Emadi, "Adjoint-based design optimization of nonlinear switched reluctance motors," *Electr. Power Compon. Syst.*, vol. 47, nos. 19–20, pp. 1705–1716, Dec. 2019, doi: 10.1080/15325008.2020.1731864.
[171] A. M. Omekanda, "Robust torque and torque-per-inertia optimization of a switched reluctance motor using the Taguchi methods," *IEEE Trans. Ind. Appl.*, vol. 42, no. 2, pp. 473–478, Mar. 2006, doi: 10.1109/TIA.2006.870031.
[172] Y. Wu and A. Wu, *Taguchi Methods for Robust Design*. Fairfield, NJ, USA: ASME Press.
[173] J. Faiz and J. W. Finch, "Aspects of design optimisation for switched reluctance motors," *IEEE Trans. Energy Convers.*, vol. 8, no. 4, pp. 704–713, 1993, doi: 10.1109/60.260984.
[174] X. Song, Y. Park, J. Li, and J. Lee, "Optimization of switched reluctance motor for efficiency improvement using response surface model and Kriging model," in *Proc. 4th Int. Joint Conf. Comput. Sci. Optim.*, Apr. 2011, pp. 259–260.
[175] J. Ma, J. Li, H. Fang, Z. Li, Z. Liang, Z. Fu, L. Xiao, and R. Qu, "Optimal design of an axial-flux switched reluctance motor with grain-oriented electrical steel," *IEEE Trans. Ind. Appl.*, vol. 53, no. 6, pp. 5327–5337, Nov. 2017, doi: 10.1109/TIA.2017.2727438.
[176] M. R. Soltanpour, H. Abdollahi, and S. Masoudi, "Optimisation of double-sided linear switched reluctance motor for mass and force ripple minimisation," *IET Sci., Meas. Technol.*, vol. 13, no. 4, pp. 509–517, Jun. 2019, doi: 10.1049/iet-smt.2018.5160.
[177] D. Wang, X. Du, D. Zhang, and X. Wang, "Design, optimization, and prototyping of segmental-type linear switched-reluctance motor with a toroidally wound mover for vertical propulsion application," *IEEE Trans. Ind. Electron.*, vol. 65, no. 2, pp. 1865–1874, Feb. 2018, doi: 10.1109/TIE.2017.2740824.
[178] F. Sahin, H. B. Ertan, and K. Leblebicioglu, "Optimum geometry for torque ripple minimization of switched reluctance motors," *IEEE Trans. Energy Convers.*, vol. 15, no. 1, pp. 30–39, Mar. 2000, doi: 10.1109/60.849113.
[179] Z.-L. Gaing, Y.-Y. Hsiah, M.-C. Tsai, M.-F. Hsieh, and M.-H. Tsai, "Hybrid design model for optimal designing of a switched reluctance motor," in *Proc. Int. Conf. Electr. Mach. Syst. (ICEMS)*, Oct. 2013, pp. 505–510.
[180] Z. Zhang, K. W. E. Cheng, N. C. Cheung, X. D. Xue, and J. K. Lin, "Design optimization of a multi-modular linear switched reluctance actuator," in *Proc. 5th Int. Conf. Power Electron. Syst. Appl. (PESA)*, Dec. 2013, pp. 1–6.
[181] A. El-Wakeel and A. C. Smith, "Optimal design of switched reluctance motors using genetic algorithms," in *Proc. Int. Conf. Elect. Mach. (ICEM)*, Bruges, Belgium, 2002, pp. 1–6.
[182] A. El-Wakeel, "Design optimisation for fault Toler ant switched reluctance motors," Ph.D. dissertation, Univ. Manchester Inst. Sci. Technol., Manchester, U.K., 2003.
[183] J. G. Amoros, P. Andrada, B. Blanque, and M. Marin-Genesca, "Influence of design parameters in the optimization of linear switched reluctance motor under thermal constraints," *IEEE Trans. Ind. Electron.*, vol. 65, no. 2, pp. 1875–1883, Feb. 2018, doi: 10.1109/TIE.2017.2686361.
[184] Y. C. Kiat, M. M. Ghazaly, S. H. Chong, and I. W. Jamaludin, "A review: Design variables optimization and control strategies of a linear switched reluctance actuator for high precision applications," *Int. J. Power Electron. Drive Syst. (IJPEDS)*, vol. 8, no. 2, p. 963, Jun. 2017, doi: 10.11591/ijpeds.v8.i2.pp963-978.
[185] F. Cupertino, G. Pellegrino, and C. Gerada, "Design of synchronous reluctance machines with multi-objective optimization algorithms," in *Proc. IEEE Energy Convers. Congr. Exposit.*, Sep. 2013, pp. 1858–1865, doi: 10.1109/ECCE.2013.6646934.
[186] J. Barta and C. Ondrusek, "Rotor design and optimization of synchronous reluctance machine," *IEEE Trans. Energy Convers.*, vol. 9, no. 2, pp. 359–365, Jun. 1994, doi: 10.17973/MMSJ.2015_03_201504.

[187] G. Pellegrino, F. Cupertino, and C. Gerada, "Barriers shapes and minimum set of rotor parameters in the automated design of synchronous reluctance machines," in *Proc. Int. Electric Mach. Drives Conf.*, May 2013, pp. 1204–1210.

[188] S. Sato, T. Sato, and H. Igarashi, "Topology optimization of synchronous reluctance motor using normalized Gaussian network," *IEEE Trans. Magn.*, vol. 51, no. 3, pp. 1–4, Mar. 2015, doi: 10.1109/TMAG.2014.2359679.

[189] M. P. Bendsøe, "Optimal shape design as a material distribution problem," *Struct. Optim.*, vol. 1, no. 4, pp. 193–202, 1989, doi: 10.1007/BF01650949.

[190] J.-K. Byun and S.-Y. Hahn, "Topology optimization of switched reluctance motor using mutual energy method," *Int. J. Appl. Electromagn. Mech.*, vol. 13, nos. 1–4, pp. 421–426, Dec. 2002.

[191] J. Yoo, "Reduction of vibration caused by magnetic force in a switched reluctance motor by topology optimization," *J. Appl. Mech.*, vol. 69, no. 3, pp. 380–387, May 2002.

[192] J. Lee, J. H. Seo, and N. Kikuchi, "Topology optimization of switched reluctance motors for the desired torque profile," *Struct. Multidisciplinary Optim.*, vol. 42, no. 5, pp. 783–796, 2010, doi: 10.1115/1.1467093.

[193] E. M. Dede, J. Lee, and T. Nomura, *Multiphysics Simulation: Electromechanical System Applications and Optimization*, Berlin, Germany: Springer-Verlag, 2015.

[194] D. Brackett, I. Ashcroft, and R. Hague, "Topology optimization for additive manufacturing of switched reluctance machines," in *Proc. 18th Biennial IEEE Conf. Electromagn. Field Comput. (CEFC)*, Oct. 2018, pp. 348–362.

[195] A. Manninen, J. Keranen, J. Pippuri-Makelainen, T. Riipinen, S. Metsa-Kortelainen, and T. Lindroos, "Impact of topology optimization problem setup on switched reluctance machine design," in *Proc. 22nd Int. Conf. Comput. Electromagn. Fields (COMPUMAG)*, Jul. 2019, pp. 1–4.

[196] Y. S. Kim and I. H. Park, "Topology optimization of rotor in synchronous reluctance motor using level set method and shape design sensitivity," *IEEE Trans. Appl. Supercond.*, vol. 20, no. 3, pp. 1093–1096, Jun. 2010, doi: 10.1109/TASC.2010.2040725.

[197] K. Watanabe, T. Suga, and S. Kitabatake, "Topology optimization based on the ON/OFF method for synchronous motor," *IEEE Trans. Magn.*, vol. 54, no. 3, pp. 1–4, Mar. 2018, doi: 10.1109/TMAG.2017.2751653.

[198] J. Lee, "Structural design optimization of electric motors to improve torque performance," Ph.D. dissertation, Univ. Michigan, Ann Arbor, MI, USA, 2010.

[199] Y. Okamoto, R. Hoshino, S. Wakao, and T. Tsuburaya, "Improvement of torque characteristics for a synchronous reluctance motor using MMA-based topology optimization method," *IEEE Trans. Magn.*, vol. 54, no. 3, pp. 2018–2021, Nov. 2018, doi: 10.1109/TMAG.2017.2762000.

[200] S. Liu, Q. Li, J. Liu, W. Chen, and Y. Zhang, "A realization method for transforming a topology optimization design into additive manufacturing structures," *Engineering*, vol. 4, no. 2, pp. 277–285, Apr. 2018, doi: 10.1016/j.eng.2017.09.002.

[201] F. Zhao and R. Yan, "Topology optimization of magnetic actuator using the improved ON/OFF method," in *Proc. 6th Int. Conf. Electromagn. Field Problems Appl.*, Jun. 2012, pp. 1–4.

[202] Y. Okamoto, K. Akiyama, and N. Takahashi, "3-D topology optimization of single-pole-type head by using design sensitivity analysis," *IEEE Trans. Magn.*, vol. 42, no. 4, pp. 1087–1090, Apr. 2006, doi: 10.1109/TMAG.2006.871422.

[203] T. Ishikawa, K. Nakayama, N. Kurita, and F. P. Dawson, "Optimization of rotor topology in PM synchronous motors by genetic algorithm considering cluster of materials and cleaning procedure," *IEEE Trans. Magn.*, vol. 50, no. 2, pp. 637–640, Feb. 2014, doi: 10.1109/TMAG.2013.2282365.

[204] Y. Okamoto, Y. Tominaga, S. Wakao, and S. Sato, "Topology optimization of rotor core combined with identification of current phase angle in IPM motor using multistep genetic algorithm," *IEEE Trans. Magn.*, vol. 50, no. 2, pp. 725–728, Feb. 2014, doi: 10.1109/TMAG.2013.2285580.

[205] T. Sato, K. Watanabe, and H. Igarashi, "A modified immune algorithm with spatial filtering for multiobjective topology optimisation of electromagnetic devices," *Int. J. Comput. Math. Elect.*, vol. 33, no. 3, pp. 821–833, 2014.

[206] T. Sato, K. Watanabe, and H. Igarashi, "Multimaterial topology optimization of electric machines based on normalized Gaussian network," *IEEE Trans. Magn.*, vol. 51, no. 3, pp. 3–6, Apr. 2015, doi: 10.1108/COMPEL-09-2012-0174.

[207] F. Shiyang and K. Watanabe, "Topology optimization of rotor design in switched reluctance motor using immune algorithm," *Int. J. Appl. Electromagn. Mech.*, vol. 2020, pp. 1–8, Sep. 2020, doi: 10.3233/JAE-209347.

[208] H. Sasaki and H. Igarashi, "Topology optimization accelerated by deep learning," *IEEE Trans. Magn.*, vol. 55, no. 6, pp. 1–5, Mar. 2019, doi: 10.1109/TMAG.2019.2901906.

[209] A. Manninen, J. Keränen, J. Pippuri-Mäkeläinen, S. Metsä-Kortelainen, T. Riipinen, and T. Lindroos, "Topology optimization of 3D printed switched reluctance motor," in *Proc. NAFEMS Nordic Seminar, Exploring Design Freedom Additive Manuf. Through Simulation*, 2018, pp. 1–12.

[210] S. Lammers, G. Adam, H. J. Schmid, R. Mrozek, R. Oberacker, M. J. Hoffmann, F. Quattrone, and B. Ponick, "Additive manufacturing of a lightweight rotor for a permanent magnet synchronous machine," in *Proc. 6th Int. Electric Drives Prod. Conf. (EDPC)*, Nov. 2016, pp. 41–45.

[211] G. M. Tseng, K. J. Jhong, M. C. Tsai, P. W. Huang, and W. H. Lee, "Application of additive manufacturing for low torque ripple of 6/4 switched reluctance motor," in *Proc. 19th Int. Conf. Electr. Mach. Syst. (ICEMS)*, Nov. 2016, pp. 15–18.

[212] T. Riipinen, S. Metsa-Kortelainen, T. Lindroos, J. S. Keranen, A. Manninen, and J. P. Makelainen, "Properties of soft magnetic Fe-Co-V alloy produced by laser powder bed fusion," *Rapid Prototyping J.*, vol. 25, pp. 699–707, Mar. 2019, doi: 10.1108/RPJ-06-2018-0136.

[213] T. Labbe and B. Dehez, "Topology optimization method based on the Maxwell stress tensor for the design of ferromagnetic parts in electromagnetic actuators," *IEEE Trans. Magn.*, vol. 47, no. 9, pp. 2188–2193, Sep. 2011, doi: 10.1109/TMAG.2011.2138151.

[214] M. Tahkola, J. Keranen, D. Sedov, M. F. Far, and J. Kortelainen, "Surrogate modeling of electrical machine torque using artificial neural networks," *IEEE Access*, vol. 8, pp. 220027–220045, 2020.

[215] R. H. Myers, D. C. Montgomery, and C. M. Anderson-Cook, *Response Surface Methodology: Process And Product Optimization Using Designed Experiments*, 3rd ed. Hoboken, NJ, USA: Wiley, 2009.

[216] Y. Duan and D. M. Ionel, "A review of recent developments in electrical machine design optimization methods with a permanent-magnet synchronous motor benchmark study," *IEEE Trans. Ind. Appl.*, vol. 49, no. 3, pp. 1268–1275, May/Jun. 2013, doi: 10.1109/TIA.2013.2252597.

[217] S. Xiao, M. Rotaru, and J. K. Sykulski, "Adaptive weighted expected improvement with rewards approach in Kriging assisted electromagnetic design," *IEEE Trans. Magn.*, vol. 49, no. 5, pp. 2057–2060, May 2013, doi: 10.1109/TMAG.2013.2240662.

[218] G. Crevecoeur, L. Dupr, and R. Van de Walle, "Space mapping optimization of the magnetic circuit of electrical machines including local material degradation," *IEEE Trans. Magn.*, vol. 43, no. 6, pp. 2609–2611, Jun. 2007, doi: 10.1109/TMAG.2007.893409.

[219] S. Shimokawa, H. Oshima, K. Shimizu, Y. Uehara, J. Fujisaki, A. Furuya, and H. Igarashi, "Fast three-dimensional optimization of magnetic cores for loss and volume Reduction," in *Proc. IEEE Int. Magn. Conf. (INTERMAG)*, Apr. 2018, pp. 2018–2021.

[220] S. Metsä-Kortelainen, T. Lindroos, M. Savolainen, A. Jokinen, A. Revuelta, A. Pasanen, K. Ruusuvuori, and J. Pippuri. *Manufacturing of Topology Optimized Soft Magnetic Core Through 3D Printing*. VTT Technical Research Centre of Finland Ltd. [Online]. Available: https://laserstatics.com/publications/metal-3d-printing-tech-01/pages/manufacturing-topology-optimized-soft-magnetic-core-through-3d-printing-001.htm

[221] H. Zhang and S. Wang, "Topology optimization of rotor pole in switched reluctance motor for minimum torque ripple," *Electr. Power Compon. Syst.*, vol. 45, no. 8, pp. 905–911, May 2017, doi: 10.1080/15325008.2017.1310769.

[222] H. Sasaki and H. Igarashi, "Topology optimization of IPM motor with aid of deep learning," *Int. J. Appl. Electromagn. Mech.*, vol. 59, no. 1, pp. 87–96, Mar. 2019.

[223] J. Asanuma, S. Doi, and H. Igarashi, "Transfer learning through deep learning: Application to topology optimization of electric motor," *IEEE Trans. Magn.*, vol. 56, no. 3, pp. 1–4, Mar. 2020.

[224] D. Zhong, Y. Yang, and X. Du, "Palmprint recognition using Siamese network," in *Proc. Chin. Conf. Biometric Recognit.*, Urumqi, China, 2018, pp. 48–55.

[225] S. Doi, H. Sasaki, and H. Igarashi, "Multi-objective topology optimization of rotating machines using deep learning," *IEEE Trans. Magn.*, vol. 55, no. 6, pp. 1–5, Jun. 2019.

**MOHAMED ABDALMAGID** (Graduate Student Member, IEEE) received the B.Sc. degree (Hons.) in electrical engineering from the Shoubra Faculty of Engineering, Benha University, Benha, Egypt, in 2011, and the M.Sc. degree in electrical engineering from the Faculty of Engineering, Cairo University, Giza, Egypt, in 2017. He is currently pursuing the Ph.D. degree in electrical engineering with the McMaster Automotive/Aerospace Resource Centre, McMaster University, Hamilton, ON, Canada.

He was a Research Assistant at the Electronics Research Institute, Cairo, Egypt, from 2013 to 2018. He is involved in many industrial projects where he designs and tests various configurations of axial flux permanent magnet motor for aerospace propulsion application. His research interests include axial flux permanent magnet (PM) motor design, switched reluctance motor (SRM) design, and optimization of SRM design for automotive/aerospace applications.

Mr. Abdalmagid also serves as a Reviewer for the IEEE TRANSACTIONS ON TRANSPORTATION ELECTRIFICATION.

**EHAB SAYED** (Member, IEEE) received the B.Sc. degree (Hons.) in electrical engineering and the M.Sc. degree in electrical engineering, electrical machines and drive systems specialization from the Shoubra Faculty of Engineering, Benha University, Egypt, in 2010 and 2016, respectively, and the Ph.D. degree in electrical engineering from McMaster University, Hamilton, ON, Canada, in 2019. From 2012 to 2016, he worked as a Teaching and Research Assistant with Benha University. While pursuing the degree, he was involved in many industrial projects where he designed various types of electric machines for different applications. He worked as a Postdoctoral Fellow at the McMaster Automotive/Aerospace Resource Centre. He is currently a Principal Engineer at Enedym Inc., Hamilton, where his focus is the design and drive of switched reluctance machines. His research interest includes design of electric machines for automotive/aerospace applications.

**MOHAMED H. BAKR** (Senior Member, IEEE) received the B.Sc. degree (Hons.) in electronics and communications engineering and the master's degree in engineering mathematics from Cairo University, Egypt, in 1992 and June 1996, respectively, and the Ph.D. degree from the Department of Electrical and Computer Engineering, McMaster University, Hamilton, ON, Canada, in September 2000. In 1997, he was a Student Intern with Optimization Systems Associates (OSA) Inc. From 1998 to 2000, he worked as a Research Assistant with the Simulation Optimization Systems (SOS) Research Laboratory, McMaster University. In November 2000, he joined the Computational Electromagnetics Research Laboratory (CERL), University of Victoria, Victoria, BC, Canada, as an NSERC Postdoctoral Fellow. He is currently working as a Professor with the Department of Electrical and Computer Engineering, McMaster University. He is the author/coauthor of over 270 journals and conference papers, two books on the optimization and CAD of high frequency structures, three book chapters on optimization, electromagnetic modeling, and artificial intelligence and two patents. His research interests include optimization methods, computational electromagnetics, computer-aided design and modeling of power circuits and motors, microwave circuits, THz, and photonic devices, nanotechnology, artificial intelligence and its applications, smart analysis of high frequency structures, and efficient optimization using time/frequency domain methods. He received the Premier's Research Excellence Award (PREA) from the province of Ontario, Canada, in 2003. He also received an NSERC Discovery Accelerator Supplement (DAS) Award in 2011. In 2014, he was a co-recipient of Chrysler's Innovation Award for project on novel designs of hybrid cars. Since 2015, he was listed on the Dean's Teaching Honor Roll several times in recognition of his success in utilizing flipped classrooms to teaching engineering courses. He was awarded in April 2018 a Leadership in Teaching and Learning (LTL) Fellowship from the McPherson Institute, McMaster University. In 2020, he was a recipient of the Faculty Appreciation Award by the McMaster Engineering Society (MES). In April 2021, he was awarded the President's Award for Outstanding Contributions for Teaching and Learning from McMaster University. He was also included in Stanford's list of the top 2% most cited scientists for 2020.

**ALI EMADI** (Fellow, IEEE) received the B.S. and M.S. degrees (Hons.) in electrical engineering from the Sharif University of Technology, Tehran, Iran, in 1995 and 1997, respectively, and the Ph.D. degree in electrical engineering from Texas A&M University, College Station, TX, USA, in 2000. He is currently the Canada Excellence Research Chair Laureate at McMaster University, Hamilton, ON, Canada. He is also the Holder of the NSERC/FCA Industrial Research Chair in Electrified Powertrains and a Tier I Canada Research Chair in Transportation Electrification and Smart Mobility. Before joining McMaster University, he was the Harris Perlstein Endowed Chair Professor of engineering and the Director of the Electric Power and Power Electronics Center and Grainger Laboratories, Illinois Institute of Technology, Chicago, IL, USA, where he established research and teaching facilities as well as courses in power electronics, motor drives, and vehicular power systems. He was the Founder, the Chairperson, and the President of Hybrid Electric Vehicle Technologies, Inc. (HEVT)–a university spin-off company of Illinois Tech. He is also the President and the Chief Executive Officer of Enedym Inc. and Menlolab Inc.—two McMaster University spin-off companies. He is the principal author/coauthor of over 500 journals and conference papers as well as several books including *Vehicular Electric Power Systems* (2003), *Energy Efficient Electric Motors* (2004), *Uninterruptible Power Supplies and Active Filters* (2004), *Modern Electric, Hybrid Electric, and Fuel Cell Vehicles* (2nd edition, 2009), and *Integrated Power Electronic Converters and Digital Control* (2009). He is also the Editor of the *Handbook of Automotive Power Electronics and Motor Drives* (2005) and *Advanced Electric Drive Vehicles* (2014). He is the Co-Editor of the *Switched Reluctance Motor Drives* (2018). He was the Inaugural General Chair of the 2012 IEEE Transportation Electrification Conference and Expo (ITEC) and has chaired several IEEE and SAE conferences in the areas of vehicle power and propulsion. He was the Founding Editor-in-Chief of the IEEE TRANSACTIONS ON TRANSPORTATION ELECTRIFICATION, from 2014 to 2020.